

An experimental study of round jets in cross-flow

By R. M. KELSO†, T. T. LIM‡ AND A. E. PERRY

Department of Mechanical and Manufacturing Engineering, The University of Melbourne,
Parkville, Victoria, Australia, 3052

(Received 14 October 1994 and in revised form 10 August 1995)

The structure of round jets in cross-flow was studied using flow visualization techniques and flying-hot-wire measurements. The study was restricted to jet to free-stream velocity ratios ranging from 2.0 to 6.0 and Reynolds numbers based on the jet diameter and free-stream velocity in the range of 440 to 6200.

Flow visualization studies, together with time-averaged flying-hot-wire measurements in both vertical and horizontal sectional planes, have allowed the mean topological features of the jet in cross-flow to be identified using critical point theory. These features include the horseshoe (or necklace) vortex system originating just upstream of the jet, a separation region inside the pipe upstream of the pipe exit, the roll-up of the jet shear layer which initiates the counter-rotating vortex pair and the separation of the flat-wall boundary layer leading to the formation of the wake vortex system beneath the downstream side of the jet.

The topology of the vortex ring roll-up of the jet shear layer was studied in detail using phase-averaged flying-hot-wire measurements of the velocity field when the roll-up was forced. From these data it is possible to examine the evolution of the shear layer topology. These results are supported by the flow visualization studies which also aid in their interpretation.

The study also shows that, for velocity ratios ranging from 4.0 to 6.0, the unsteady upright vortices in the wake may form by different mechanisms, depending on the Reynolds number. It is found that at high Reynolds numbers, the upright vortex orientation in the wake may change intermittently from one configuration of vortex street to another. Three mechanisms are proposed to explain these observations.

1. Introduction

The study of jets in cross-flow is of great practical relevance to both engineering applications and natural phenomena. Numerous examples can be found in aeronautics, industry and nature. These include V/STOL aircraft during transition flight, gas turbine blade cooling and exhaust gas cooling, the roll-control of missiles, chimney flows, sewerage outfalls, and many biological systems. Although some of these flows may be influenced to varying degrees by buoyancy effects, they nevertheless exhibit many features in common with the jets of neutral and low buoyancy which have been

† Current address: Department of Mechanical Engineering, The University of Adelaide, S. A., Australia, 5005.

‡ Current address: Department of Mechanical and Production Engineering, National University of Singapore, 10 Kent Ridge Crescent, Singapore 0511.

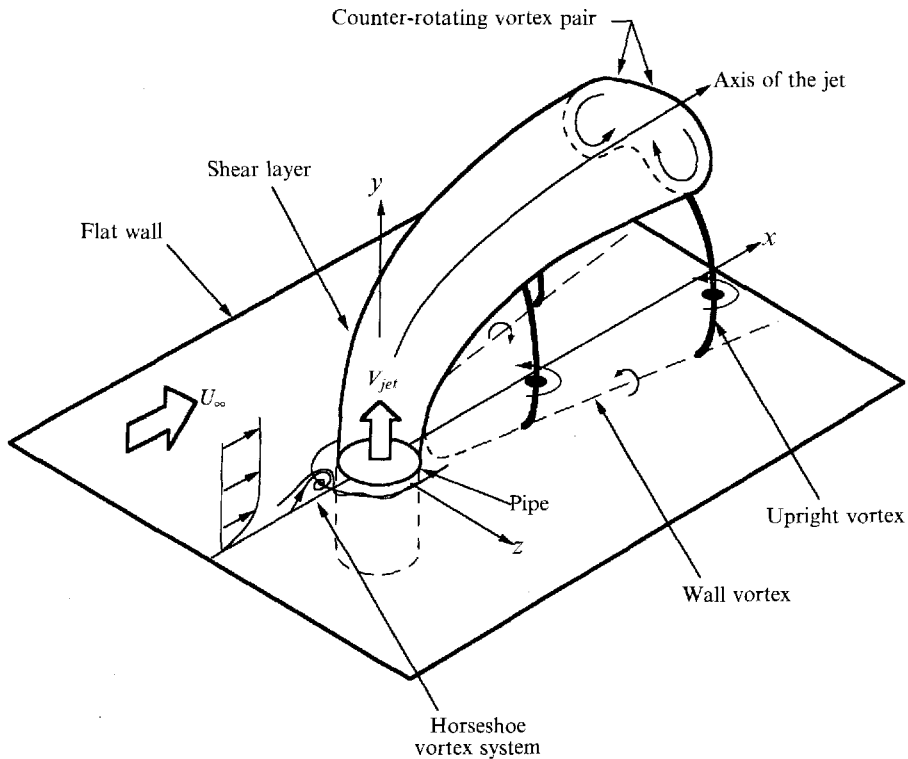


FIGURE 1. Schematic diagram showing the many vortex systems of a jet in cross-flow. Wall vortices and upright vortices are considered to be part of the 'wake' region (see text).

studied in the laboratory. This paper will focus on the resulting flow when a circular jet nozzle is mounted flush with a flat wall without buoyancy as shown in figure 1.

The characteristics of a jet in cross-flow are primarily dependent on the ratio of the momentum flux from the jet orifice to the momentum flux of the cross-flow over equal areas. It is conventional to define the 'effective velocity ratio' R as the square root of this ratio. When the jet and cross-flow densities are equal, R is often given by the approximation

$$R = V_{jet}/U_{\infty}$$

where V_{jet} is the (time-averaged) volume flux divided by the area of the jet and U_{∞} is the free-stream velocity of the cross-flow.

When a jet discharges normal to a cross-flow there is a complex interaction between the two flows, resulting in the deflection of the jet in the direction of the cross-flow. The jet flow forms a pair of counter-rotating vortices which seem to originate in the near field and dominate the flow field far downstream. The near-field structure of the shear layer consists also of ring-like or loop-like vortices which become distorted with streamwise distance. The flat-wall boundary layer forms a system of horseshoe vortices similar to the flow around a solid body attached to a wall. The wake region beneath the downstream side of the jet contains a complex system of vortices (see figure 1), consisting of the streamwise 'wall vortices' which lie above the flat wall, and vertically oriented shedding vortices, defined here as 'upright vortices'. Under some conditions the pattern of upright vortices can bear a similarity to the vortex street

downstream of a solid cylinder. In this paper the term 'wake' is used for historical reasons although this region is not a wake in its usual sense, as will be shown.

Early experimental studies focused on the mean trajectory of jets and the evolution of the flow along the mean trajectory (Keffer & Baines 1963; Kamotani & Greber 1972; Chassaing, *et al.* 1974), analytical and computational schemes to predict the velocity field and trajectories of jets (Sucec & Bowley 1976 and Patankar, Basu & Alpay 1977 respectively) and the surface pressure distributions (Bradbury & Wood 1965; McMahon & Mosher 1969; Bergeles, Gosman & Launder 1976; Andreopoulos 1982 and Kavsaoglu & Schetz 1989 to name but a few). Surface streakline patterns have been visualized by Bradbury & Wood (1965), Bergeles *et al.* (1976), Foss (1980) & Krothapalli, Lourenco & Buchlin (1990) and Krothapalli & Shih (1993).

It has long been recognized that a bent-over jet forms a counter-rotating vortex pair (henceforth referred to as CVP) which becomes the dominant flow feature and which persists far downstream (see Scorer 1958, Keffer & Baines 1963; Pratte & Baines 1967). Broadwell & Breidenthal (1984) showed that the CVP arises from the jet momentum normal to the cross-flow and that the CVP is therefore a global feature of the far field. Many experimental studies have focused on the time-averaged structure of the CVP, for example Kamotani & Greber (1972), Fearn & Weston (1974), Moussa Trischka & Eskinazi (1977) and Rajarantnam & Gangadharaiah (1983). However, the mechanism of formation of the CVP remains poorly understood. The consensus of opinion is that the CVP is formed by the vortex sheet (or thin shear layer) which emanates from the pipe, as suggested by Moussa *et al.* (1977), Coelho & Hunt (1989), Andreopoulos (1984, 1985), Andreopoulos & Rodi (1984) and Sykes, Lewellen & Parker (1986). This conclusion is further supported by Perry & Lim (1978) who described how the cylindrical vortex sheet of a buoyant co-flowing jet becomes distorted to produce streamwise vortices. Although this is a different flow case there are many similarities. Coelho & Hunt (1989) suggested that the CVP may be initiated within the pipe itself, a suggestion which has been supported by velocity profile measurements (see Bergeles *et al.* 1976; Crabb, Durao & Whitelaw 1981 and Andreopoulos 1982). Fric (1990) compared the flux of vorticity from the nozzle with the flux of vorticity in the fully developed counter-rotating vortices and concluded that it is possible for the CVP to evolve from the vorticity emanating from the jet nozzle, and that it may do so within the near field.

Horseshoe vortices (or necklace vortices) have been observed around jets in cross-flow. Krothapalli *et al.* (1990) studied the horseshoe vortex system upstream of a rectangular jet in cross-flow, observing two distinct regimes of behaviour with changing velocity ratio. They observed that the formation and roll-up of the horseshoe vortices can be a periodic phenomenon which occurs at a frequency similar to the periodic vortices in the wake. Kelso & Smits (1995) also observed unsteady horseshoe vortex systems in the case of a round jet in cross-flow. They found that different regimes of unsteadiness are possible and that these motions may be coupled to the periodic motions of the upright vortices in the wake. Andreopoulos (1982) also observed a horseshoe vortex system, as well as a separation region occurring intermittently inside the jet nozzle when $R = 0.5$. Some further observations of the horseshoe vortices were made by Fric & Roshko (1989, 1994), Fric (1990), Shang *et al.* (1989) and Krothapalli & Shih (1993).

The structure of the wake region has been studied by relatively few workers (see McMahon, Hester & Palfrey 1971; Moussa *et al.* 1977; Kuzo & Roshko 1984; Wu, Vakili & Yu 1988). Unfortunately, none of this work led to a conclusion as

to the source of the vorticity in the wake region or the mechanism by which the upright vortices are formed. However, in a recent study Fric & Roshko (1989, 1994) and Fric (1990) pointed out that, as suggested by Lighthill (1963) and Morton (1984), in a flow of uniform density, vorticity cannot be generated away from solid boundaries. Therefore, the vortices in the wake region must result from the convection, turning, stretching and diffusion of vorticity generated at the flat wall and/or nozzle boundaries. Fric & Roshko's flow visualization studies confirmed that the vorticity in the wake region originates in the flat-wall boundary layer. They observed that the boundary layer fluid outside the horseshoe vortices 'wraps around the jet and then separates on its lee side....' They described 'separation events' which occur periodically, alternating from one side of the jet to the other, leading to the observed upright vortices. Fric & Roshko suggested that the strong adverse pressure gradient encountered by the boundary layer around the rear side of the jet is consistent with the observed boundary layer separation events. Spectral measurements also showed that the frequency of the separation events is very close to the frequency of the upright vortices, which supports their conclusions.

The purpose of this work is to take a fresh look at jets in cross-flow using newly developed tools, both theoretical and experimental, such as topological techniques with the associated critical point theory and the flying-hot-wire apparatus. Two studies were carried out. One was a flow visualization study in a water channel and the other was a flying-hot-wire study in a wind tunnel. To enable direct comparison with the hot-wire measurements, limited smoke visualization studies were also conducted in the same wind tunnel. This paper is organized as follows. In §2 we discuss the experimental facilities and techniques. Section 3 describes the behaviour of the jet shear layer and horseshoe vortex system using results obtained from dye visualization experiments in a water channel and smoke visualization and hot-wire anemometry experiments in a wind tunnel. In §4 the surface and sectional streamline patterns are visualized and interpreted from both dye visualization studies and hot-wire measurements. Section 5 describes the behaviour of the upright vortices in the wake region and proposes three possible mechanisms leading to the observed behaviour. Section 6 then summarizes the results and presents some concluding remarks.

The terminology used here for the topological descriptions is that used by Perry & Fairlie (1974) and Perry & Chong (1987).

2. Experimental apparatus and methods

2.1. Water channel experiments

Flow visualization experiments were carried out in the closed-return water channel at the University of Melbourne. A detailed description of this apparatus is given in Kelso (1991). Figure 2 shows a schematic diagram of the apparatus. The pipe had an internal diameter of 25 mm which was chosen to achieve geometric similarity with the wind tunnel apparatus. The pipe was very short ($3.5D$ in length), with the fluid entering it from an axisymmetric 36:1 contraction, thus giving a top-hat velocity profile in the case of no cross-flow. The jet's water supply was isolated from the main channel circuit by a constant-head tank. The Reynolds number Re and velocity ratio R are defined in figure 2. The flat-wall boundary layer profile upstream of the pipe was laminar, with a thickness varying between 12 mm ($\delta/D = 0.47$) and 32 mm ($\delta/D = 1.3$) over the range of Reynolds numbers considered.

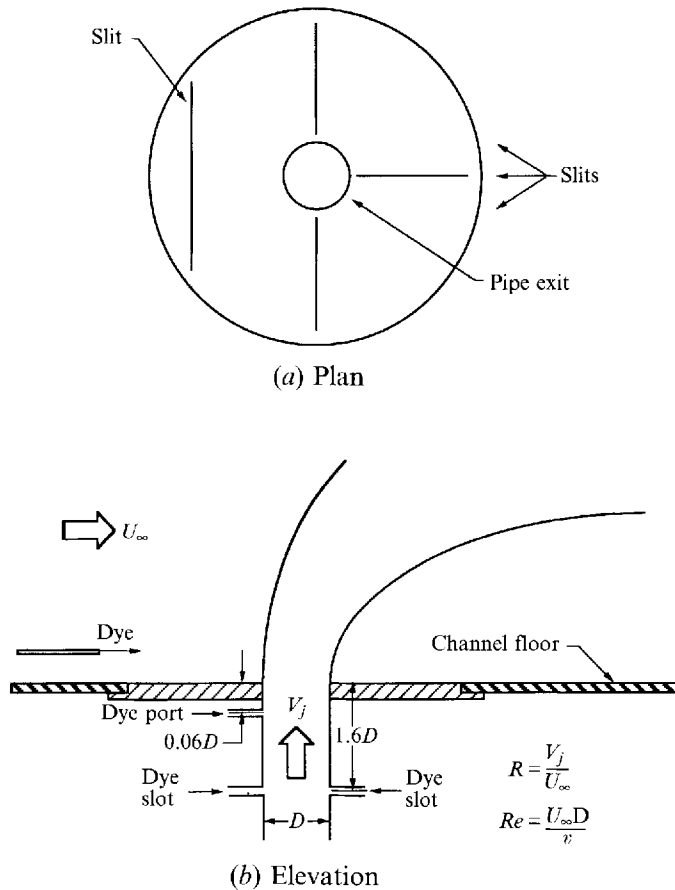


FIGURE 2. Schematic diagram of the jet apparatus.

A narrow circumferential slot in the pipe wall allowed dye to be injected directly into the pipe boundary layer (hence the jet shear layer). A small dye injection port was also located in the pipe wall immediately upstream of the exit. The pipe was mounted in a disc which fitted neatly into a circular hole in the floor of the channel. The disc could be rotated to any desired angle. Four dye injection slits were incorporated into the face of the disc, allowing dye to be injected into the channel floor boundary layer at different locations. Moveable dye injection tubes were also used to introduce dye into the cross-flow from points away from the wall. Dyes with specific gravity 1 were used to visualize the flow.

To avoid the possibility of erroneous interpretation of the streakline patterns (see for example Gursul, Lusseyran & Rockwell 1990) the dyes were, where possible, introduced from the injection slot, slits and port a short distance ahead of any shear layer separation. In such cases, the diffusion of dye and momentum near the wall is governed by the molecular Schmidt number which is of the order of 10^3 (see Goldstein & Smits 1994). Therefore the rate of diffusion of vorticity is many times greater than the rate of diffusion of the dye. Hence, dye introduced in this way will accurately mark the shear layer at separation and will generally speaking distribute itself about the centroids of vorticity. This is illustrated in the experiments of Perry & Tan (1984) in co-flowing jets and wakes. Thus, in the dye visualization experiments

described in this paper, the diffusion of vorticity and dye can be considered to be almost coincident for short times. Nevertheless, the differential diffusion of the dye and vorticity increases with time (or distance from the dye source) and also increases as the Reynolds number is decreased. In cases where the flow features were visualized by dye introduced from the moveable dye injection tubes, the existence of each feature was confirmed by introducing dyes in different ways and from different locations.

2.2. Wind tunnel experiments

The wind tunnel experiments were carried out in the Large Flow Visualization Wind Tunnel at the University of Melbourne. The tunnel has a working section measuring $1.2 \text{ m} \times 0.9 \text{ m}$ and is equipped with a flying-hot-wire apparatus. This facility, which is described in Kelso, Lim & Perry (1994), was required because the jet in cross-flow involves eddying motions which cause large changes in the velocity vector directions and regions of reversed flow. Successful hot-wire anemometry can be accomplished only with the aid of a flying-hot-wire system of this type.

A round pipe of diameter $D = 95.5 \text{ mm}$ was mounted in the floor of the working section and aligned normal to the tunnel flow. An axisymmetric, radial air intake with a contraction ratio of 18:1 was attached to the pipe inlet. The floor of the radial intake incorporated a membrane with a central solid conical section which could be made to oscillate with a small amplitude, causing a controlled fluctuation in the jet velocity. This mechanism was used to force the shear layer of the jet to roll up at a known frequency. Velocity measurements were sorted and averaged on the basis of the phase of the forcing input. Unforced cases are mentioned later. The free-stream velocity for both forced and unforced cases was 1.0 m s^{-1} with an average jet velocity of 2.2 m s^{-1} , giving $R = 2.2$ and a Reynolds number of 6200. No boundary layer tripping devices were used in either the wind tunnel or the pipe. The upstream boundary layer profile in the wind tunnel was laminar, with a thickness of 27 mm ($\delta/D = 0.28$). In the absence of cross-flow, the pipe gave a top-hat velocity profile at its exit. A detailed description of this apparatus and the flow conditions can be found in Kelso (1991).

Time-averaged vector fields of the unforced flow were measured in the vertical centre-plane and a horizontal plane located 40 mm ($y/D = 0.42$) above the floor of the wind tunnel. The velocity data at each point were averaged over 400 passes of the hot-wire probe. The hot-wire signals were low-pass filtered with a cut-off frequency of 10 kHz. The horizontal-plane measurements were accomplished by traversing the jet sideways, since the flying-hot-wire system did not allow the probe to be traversed in the z -direction (as defined in figure 1).

In the forced flow, the phase-averaged measurements of the velocity components in the vertical centre-plane were averaged over 400 passes. The data were sampled and sorted on the basis of the phase of the forcing input using 16 equal phase intervals. To increase the rate of convergence of the data, the hot-wire signals were low-pass filtered at a cut-off frequency of 1 kHz.

The software and methods used to acquire and process the data in these experiments are described in Kelso *et al.* (1994). All velocity data were three-point smoothed along both the rows and columns of the data grid. Streamline patterns were computed using a modified predictor-corrector method, calculated using cubic spline interpolations of the data.

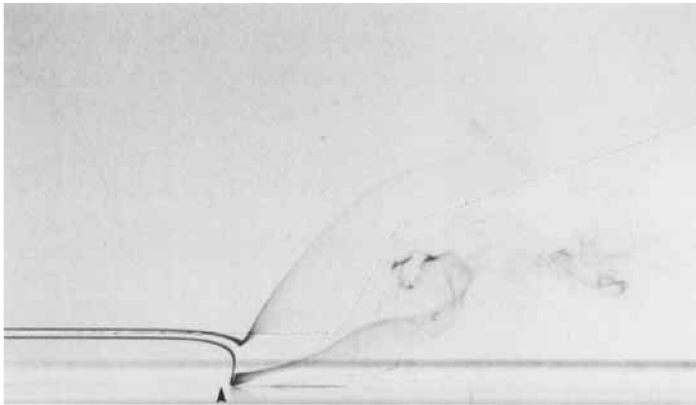


FIGURE 3. Flow pattern obtained when dye is injected from tubes located far upstream and also released from the dye injection port. $Re = 940$, $R = 2.3$ and $\delta/D = 0.81$. This figure is a composite of two dye patterns obtained in the same flow at different times. The upstream lip of the pipe is marked by an arrow head.

3. Results

3.1. Flow visualization in the water channel

3.1.1. Shear layer structure

The shear layer instability was found to form by different mechanisms, depending on the Reynolds number and velocity ratio.

Figure 3 shows the pattern obtained at $R = 2.3$ and $Re = 940$ where dye was injected from an injection tube far upstream. The photograph shows a steady vortex above the jet exit. The vortex, henceforth referred to as the 'hovering vortex', wraps around the front and sides of the jet and appears to contribute vorticity to the counter-rotating vortex pair of the jet. This is not to be confused with the horseshoe vortices located close to the flat wall. Under these conditions the hovering vortex occasionally becomes unstable and sheds a train of vortex loops or rings into the shear layer. The shear layer of the jet is laminar with a Kelvin–Helmholtz-like instability apparent at about 3 pipe diameters above the jet exit. Figure 4 shows the authors' interpretation of this flow case. Under conditions where the shear layer rolls up by a Kelvin–Helmholtz-like instability, it was found that there is no roll-up on the rear side of the jet. When the Reynolds number is gradually increased above 940, the Kelvin–Helmholtz-like instability occurs progressively closer to the jet exit until the hovering vortex itself begins to shed ring vortices periodically and flow patterns such as those in figures 5(a) and 8 are produced. Under these conditions the shear layer roll-up is of large scale, is periodic, and occurs near or within the pipe exit. One may conclude that when this periodic roll-up occurs, the hovering vortex only exists as a 'mean' or 'time-averaged' feature of the flow.

Figure 5 depicts the behaviour of the shear layer at a Reynolds number of 1600 and velocity ratios of 2.2 and 4.0. In these photographs red dye is injected from the dye port (see figure 2) into the upstream side of the pipe and blue dye is released into the boundary layer of the pipe. When dye is released from the port, it seems to fill a small separation region which occurs just below the upstream lip of the nozzle. Consequently, all the red dye seen in the photographs originates from this separation region. It must be emphasized that although the shear layer roll-ups shown in the

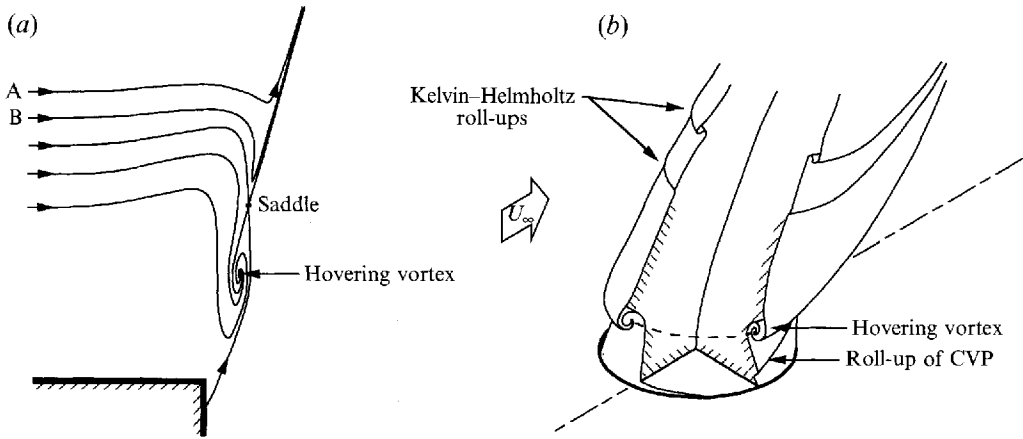


FIGURE 4. Authors' interpretation of the 'hovering vortex' at $Re = 940$, $R = 2.3$ and $\delta/D = 0.81$, showing (a) a cross-sectional view at the upstream side of the jet and (b) a cut-away perspective view of the jet.

photographs are periodic, no deliberate forcing was applied. The vortex rings are initially tilted downwards at the upstream side of the jet and, as the rings convect upwards, the plane containing the upstream part of the rings rotates clockwise such that the plane is always approximately normal to the axis of the jet. Pairing of the ring-like vortices occurs on the upstream side of the jet. This behaviour was observed at all velocity ratios considered in this paper, although vortex pairing occurs less frequently and further from the pipe exit at the lower velocity ratios. No pairing was observed on the downstream side. The figures also show the correspondence between the roll-ups marked red at the front and sides of the jet and the roll-ups marked blue at the downstream side. This is confirmed by video recordings of the flow and implies that under these conditions the ring-like vortices form by a roll-up of the shear layer around the entire perimeter of the jet (cf. Perry & Lim 1978 in which similar structures in co-flowing jets do not roll-up on what was effectively the downstream side). The photographs also show the gradual 'collapse' of the rings as the upstream and downstream sides meet, defining the end of the core region of the jet.

A significant feature of the flow pattern is revealed by this experiment, namely the initiation of the CVP. Figure 5 shows that the shear layer of the jet folds (see label) and rolls up very near to the pipe exit, leading to or contributing to the formation of the CVP. The correspondence between the folds and the interface between the red and blue dyes suggests that there is a connection between the CVP roll-up and the separation inside the pipe. Furthermore, although the blue dye is injected evenly into the pipe boundary layer all around the circumference, most of the dye is swept to the downstream side of the jet, indicating a substantial secondary flow in the pipe boundary layer near the pipe exit.

Figure 6 shows the flow pattern obtained at $R = 5.5$ and a Reynolds number of 1600 when dye is injected from the circumferential slot in the pipe. At this velocity ratio, the separation region inside the pipe is very small and the ring-like shear layer roll-ups form a short distance above the pipe exit. Here the folding occurs closer to the upstream side of the pipe and the rolling-up of the shear layer is very rapid, leading to pronounced counter-rotating vortices on either side of the jet.



FIGURE 5. Behaviour of the jet shear layer for velocity ratios (a) 2.2 and (b) 4.0 at $Re = 1600$ and $\delta/D = 0.61$. In these photographs, blue dye is injected from the circumferential slot in the pipe and red dye is released from the dye injection port.



FIGURE 26. (See §5.) Upright vortex structure visualized by introducing red and blue dyes from radial slots in the channel floor at $Re = 2700$, $R = 4.0$ and $\delta/D = 0.47$. The slots were oriented at 45° from the centre-line on the downstream side of the jet. Blue dye was injected on the near side and red on the far side. Photograph (a) shows alternating red and blue upright vortices and (b) shows alternating pairs of red and pairs of blue upright vortices. In both photographs, the downstream lip of the pipe is marked by an arrow head.

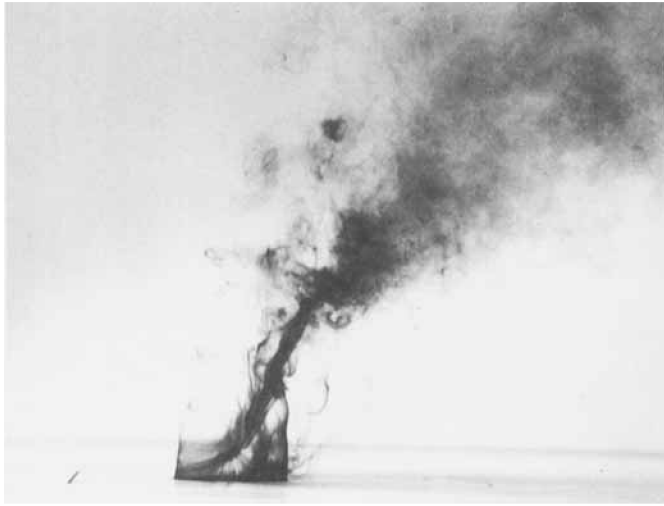


FIGURE 6. Flow pattern obtained when dye is injected from the circumferential slot in the pipe at $Re = 1600$, $R = 5.5$ and $\delta/D = 0.61$.



FIGURE 7. Close-up view of vortex breakdown in the CVP at $Re = 1600$, $R = 4.0$ and $\delta/D = 0.61$.

An unexpected phenomenon can be seen, particularly in figure 5(b) and figure 6, namely, vortex breakdown of the CVP. The phenomenon is most clearly seen at velocity ratios above 3. Figure 7 shows a close-up view of the breakdown phenomenon at $R = 4.0$. Video recordings of the breakdown indicate that there is a region of reversed flow normally associated with breakdown. The presence of this breakdown may be, in part, responsible for the effective mixing properties of this type of flow. This phenomenon is currently under investigation.

Figure 8 shows an example where a filament of dye injected from a tube upstream appears to 'stagnate' on the vortex sheet of the jet at a point resembling a half-saddle (Perry, Lim & Chong 1980). In fact, the appearance of a 'half-saddle' is probably an

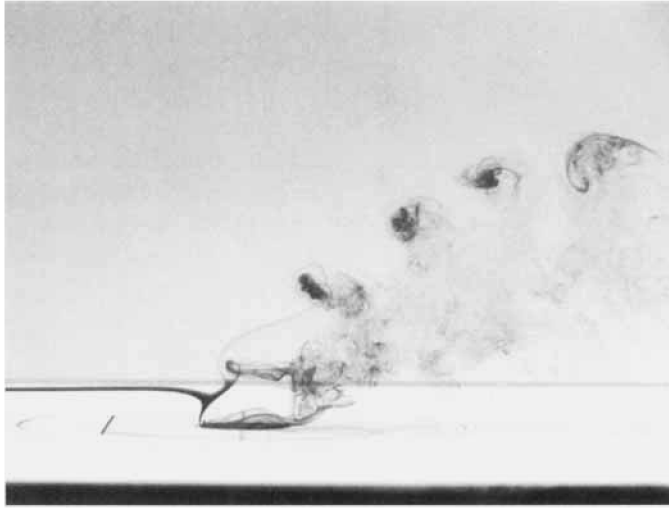


FIGURE 8. Flow pattern obtained when dye is released from the dye injection port and from a tube located far upstream. $Re = 1600$, $R = 2.2$ and $\delta/D = 0.61$.

artifact of a thick dye filament impinging on a very thin shear layer. For example, in figure 4(a), imagine the dye filling the region between streamlines A and B. When the size of the dye filament is decreased, the filament's behaviour approaches that of streamline A or B alone.

Figure 9 shows the authors' interpretation of the major roll-up processes of the jet shear layer as shown in figures 5, 6 and 8. The large-scale vortex ring-like roll-up, similar to that of a free jet, is described in figure 9(a). Figure 9(b) shows the mean reorientation of the shear layer vorticity which leads to (or contributes to) the formation of the CVP. Figure 10 shows the superposition of these two processes. This interpretation suggests that the vortex rings fold into two parts: the upstream part whose plane tilts with the mean curvature of the jet, and the downstream part whose plane becomes aligned with the direction of the jet, and so the sides of the downstream part contribute to the circulation of the CVP. Similar mechanisms have been suggested by Moussa *et al.* (1977), Andreopoulos (1985), Sykes *et al.* (1986) and others. This tilting and folding scenario is also consistent with the mechanism suggested by Perry & Lim (1978) and later developed by Perry & Tan (1984) for buoyant co-flowing jets. However, the roll-up process of jets in cross-flow is highly distorted by the presence of the other vortex systems of the flow.

3.2. Pipe separation and horseshoe vortices

The limiting surface streamline pattern of the separation inside the pipe is shown in figure 11, presented as though the pipe were split at $\theta = 180^\circ$ and opened out flat. The separation streamsurface within the pipe separates from the wall at a negative bifurcation line. This bifurcation line extends from a saddle point S at $\theta = 0^\circ$, then around the sides to the edge of the pipe. This pattern accounts for the very sharp differentiation between the red- and blue-marked regions of the shear layer shown in figure 5. It was observed that the size of the separation region decreases with increasing R . For example, at $R = 2.2$ and $Re = 1600$, the saddle point S is located at approximately $y/D = -0.4$ whereas at $R = 4.0$ and $Re = 1600$, it is located at $y/D = -0.16$. At high velocity ratios ($R > 6$) the saddle point is located at the lip.

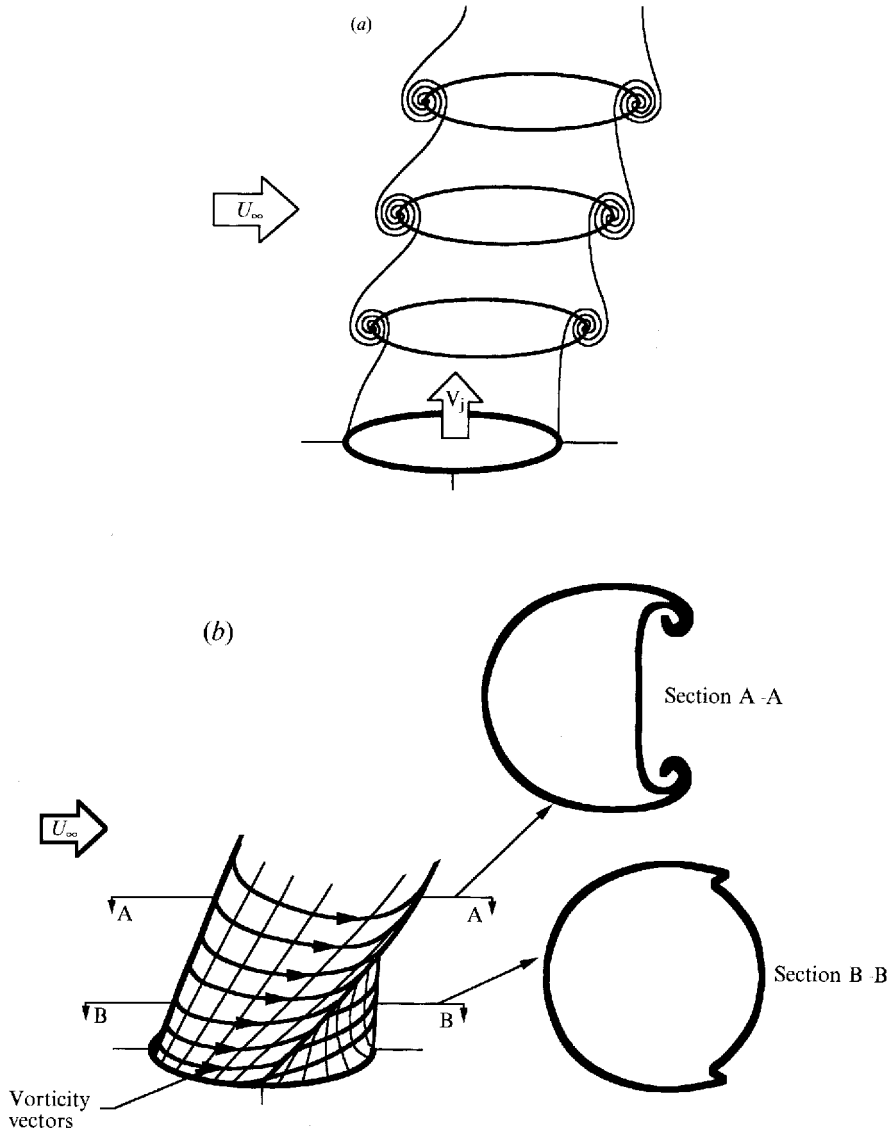


FIGURE 9. Schematic diagram showing (a) the large-scale vortex ring-like roll-up and (b) the reorientation of the shear layer vorticity leading to the folding of the cylindrical vortex sheet.

Pressure measurements carried out in the wind tunnel in independent studies (Kelso 1991 and Andreopoulos 1982) show that an adverse pressure gradient is present in the pipe on the upstream side. The available data would also suggest that this pressure gradient decreases with increasing R . These observations are entirely consistent with those of the present study.

Figure 12 shows a side view of the horseshoe vortex system induced by the jet in cross-flow for $R = 2.2$, when streaklines of dye are introduced from appropriate locations far upstream. The horseshoe vortex system shown is steady with no periodic vortex shedding observed (see Andreopoulos 1982; Fric 1990; Kelso & Smits 1995) at the flow conditions discussed in this paper, although a small oscillation of the horseshoe vortices was observed, which appears to be induced by the vortex ring

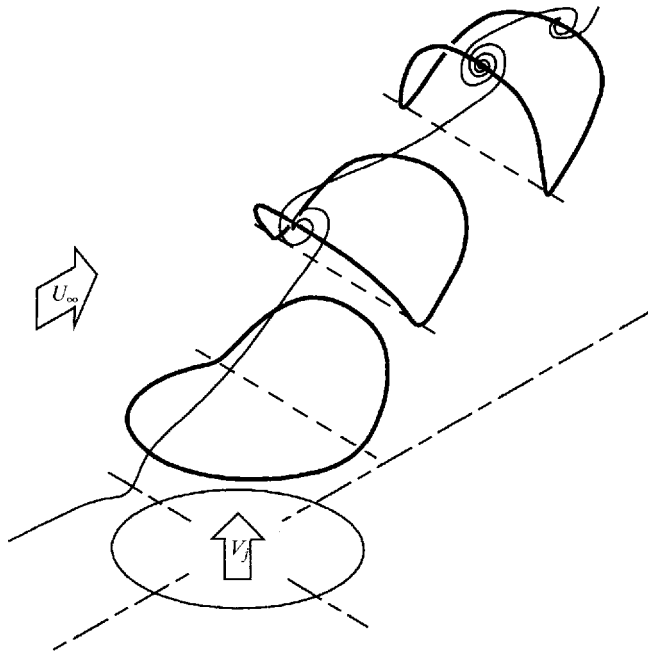


FIGURE 10. Isometric view of the authors' interpretation of the jet shear layer vortex rings, showing how they tilt and fold as they convect downstream.

instability of the jet shear layer. The behaviour of the horseshoe vortex system on the upstream side of the jet appears to be qualitatively similar over the range of Reynolds numbers (440 to 1600) and velocity ratios (1.0 to 6.0) studied by the authors. No observations of horseshoe vortices were made for $Re > 1600$. For a comprehensive discussion of horseshoe vortices, see Doligalski, Smith & Walker (1994).

The downstream trajectories of the horseshoe vortices were studied over a range of Reynolds numbers and velocity ratios. The low Reynolds number ($Re < 1000$) observations are depicted in figure 13. At low Reynolds number it was found that, on average, the horseshoe vortices having vorticity of the same sign as the flat-wall boundary layer vorticity, extend downstream along the flat wall and are incorporated into the vortex system of the wake. All the horseshoe vortices with vorticity opposite to that of the flat-wall boundary layer, are lifted away from the wall behind the jet and merge with the CVP. These interpretations also appear to be applicable, in the mean at least, to higher Reynolds number cases where upright vortices are present in the wake region.

The nature of the flow at the upstream portion of the lip of the pipe is also illustrated in figure 12 where a streakline of dye impinges on the corner of the pipe and the tunnel floor at the centre-line. The streakline was found to split with one part flowing upstream along the tunnel floor and the other part flowing down into the pipe. The dye flowing onto the tunnel floor is swept upstream into the horseshoe vortex system, whereas the dye flowing into the pipe is swept into the separation region within the pipe.

Figure 14 shows the authors' interpretation of the flow patterns in the vertical centre-plane relative to a stationary observer, inferred from both direct observation and topological arguments. The patterns consist of stable foci and saddles, where all the foci draw in or 'attract' fluid from the cross-flow. Careful observation of the

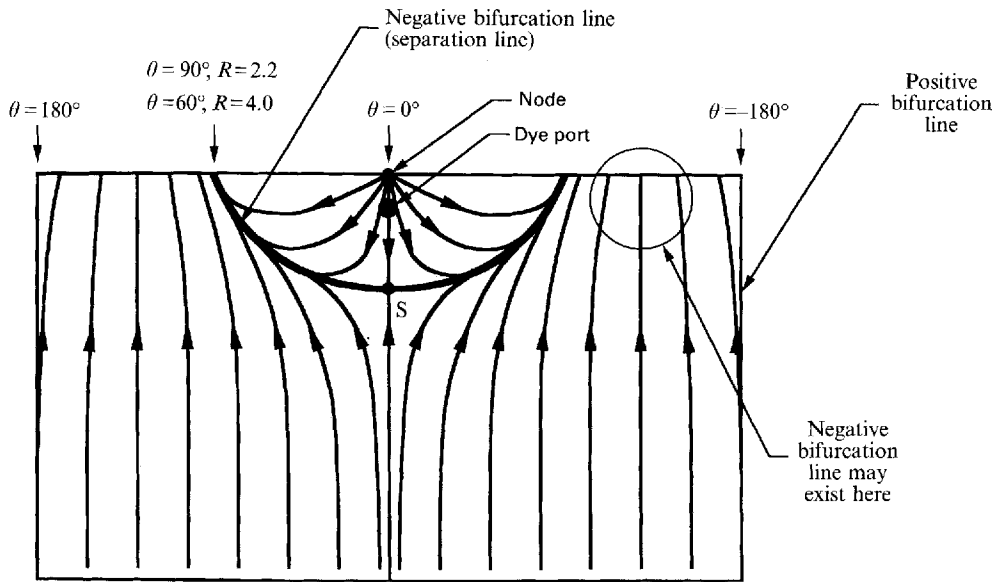


FIGURE 11. The surface streamline pattern inside the pipe, presented as though the pipe were split at $\theta = 180^\circ$ and opened out flat.

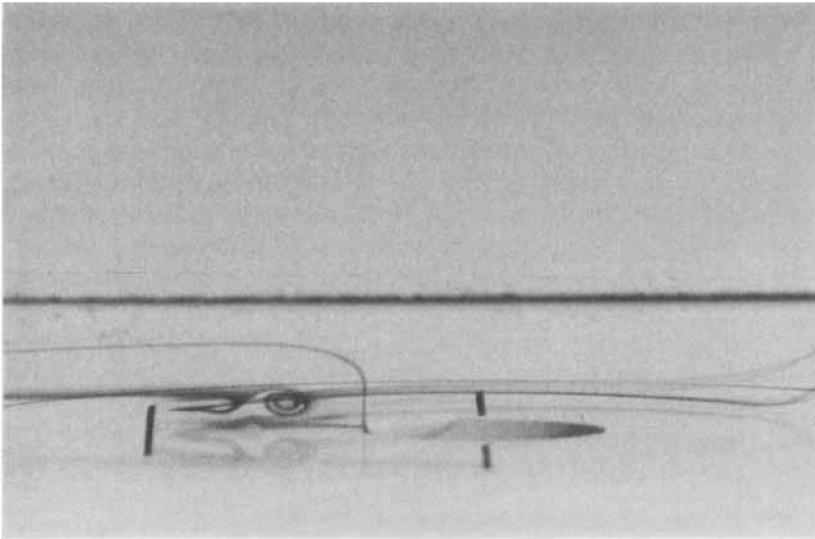


FIGURE 12. The horseshoe vortex system, visualized by dye streaks introduced from tubes located far upstream. $Re = 1600$, $R = 2.2$ and $\delta/D = 0.61$.

streakline splitting at the corner (similar to figure 12) revealed that a tiny separation region exists at the corner and that this separation region oscillates back and forth in phase with the roll-up of the jet shear layer. The two alternative flow patterns occur at different stages in the jet shear layer roll-up cycle. The authors suggest that these patterns would be similar to the time-averaged flow pattern at both higher Reynolds numbers than those considered in this study and lower Reynolds number cases where the hovering vortex occurs.

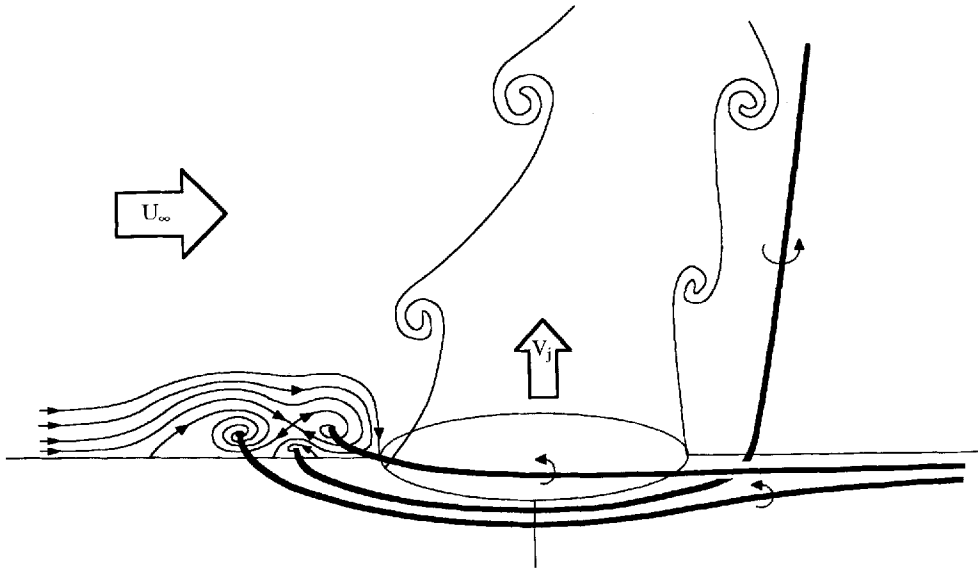


FIGURE 13. Trajectories of the horseshoe vortices at low Reynolds number.

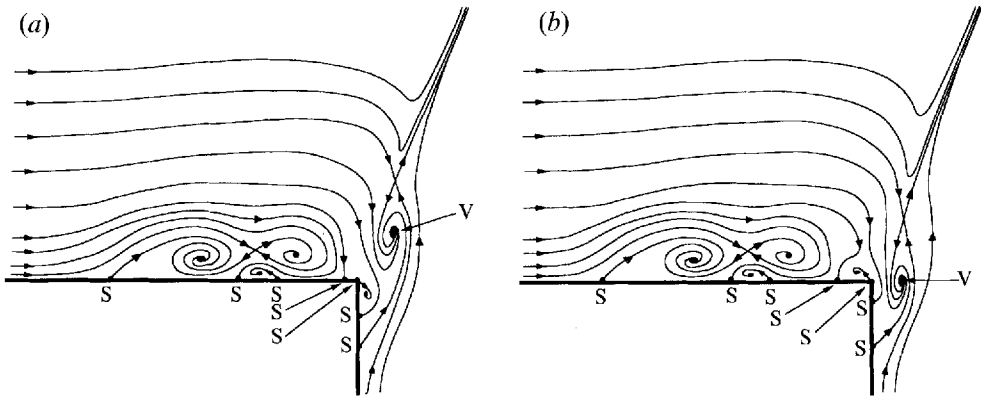


FIGURE 14. Authors' interpretation of the instantaneous streamline pattern in the vertical centre-plane as seen by a stationary observer. The shear layer vortices (V) are assumed to be moving slowly enough to be seen by a stationary observer. The two patterns show the flow topology at different stages of the jet shear layer roll-up cycle as shown by the different positions of vortex V . As the shear layer vortices roll up and convect away, the separation region at the upstream lip of the pipe oscillates between the two states shown.

3.3. Flow visualization in the wind tunnel

Flow visualization experiments were conducted so as to obtain smoke patterns for comparison with the measured velocity fields and water channel experiments. As stated earlier, the wind tunnel experiments were conducted at $R = 2.2$ and a Reynolds number of 6200, approximately four times the Reynolds number used in the comparable water channel experiments. Forcing was applied to the jet flow in the wind tunnel at 7.1 ± 0.05 Hz (Strouhal number $fD/U_\infty = 0.65$), close to the frequency of the unforced shear layer roll-up on the upstream side within $3D$ of the jet exit. The amplitude of the fluctuation was 10 % of the mean jet velocity.

Figure 15(a) shows a laser cross-section of the vertical centre-plane of the near field

(a)



(b)

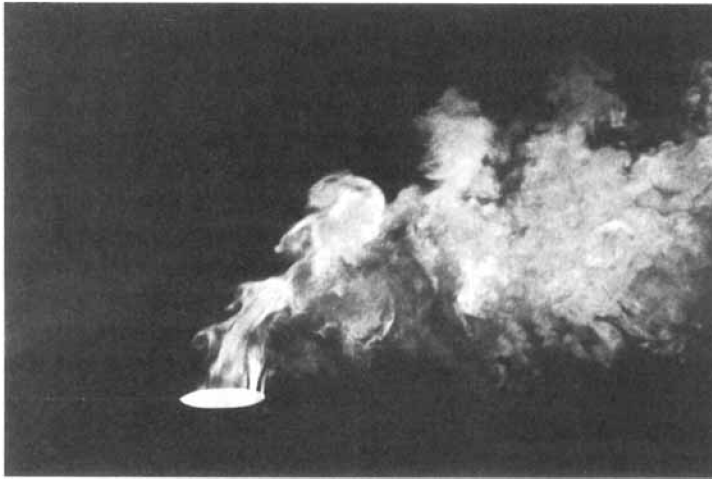


FIGURE 15. Laser cross-sections of the vertical centre-plane of the near field of the (a) unforced jet and (b) forced jet. $Re = 6200$, $R = 2.2$ and $\delta/D = 0.28$.

of the unforced jet. Smoke was injected into the jet fluid upstream of the contraction from eight equi-spaced smoke injection nozzles. The ring-like roll-up of the shear layer can be seen on the upstream side and, to a lesser extent, on the downstream side of the jet. The roll-up is periodic although regular vortex amalgamations occur on the upstream side of the jet.

Figure 15(b) shows the same jet when it was forced at 7.1 Hz. The photograph suggests that the forcing may have been at a marginally lower frequency than the natural shear layer roll-up. The forcing appears to have increased the size of the vortex rings, hence the shear layer growth rate. Note that vortex pairing occurs approximately three diameters from the jet exit whether the forcing is applied or not. In the forced case this phenomenon led to a 'washout' of the phase-averaged velocity data since the averaging was made on the basis of the external forcing input. This does not present a problem since the coherence of the eddies is consistently good within the first few diameters, leading to reasonable results being obtained close to the jet exit.

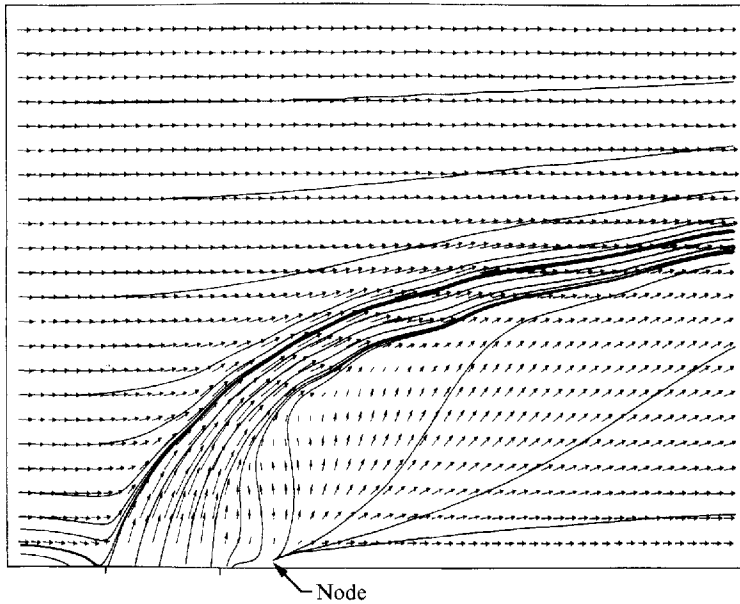


FIGURE 16. Time-averaged vector field and streamline pattern in the vertical centre-plane for the unforced jet. $Re = 6200$, $R = 2.2$ and $\delta/D = 0.28$. The pipe location is indicated by tick marks. Base of figure corresponds with wall.

3.4. Flying hot-wire studies

3.4.1. Unforced structure

Figure 16 shows the time-averaged vector field of the jet in the vertical centre-plane with the integrated streamline pattern superimposed. An extra row of experimental data (not shown), located mid-way between the flat wall and the first data level, was used to compute the streamlines near the flat wall. Below this level, the streamlines were computed from extrapolated data.

Although the flying hot wire was flown at high velocity, the pitch angle of the flow relative to the probe approached 28° in the core region of the jet, close to the pipe exit. This caused errors of up to 6% in the inferred velocities in this region. These errors have not been corrected since they do not alter the topology of the time-averaged flow field in any way.

An unexpected feature of figure 16 is the waviness of the streamlines, particularly in the region of the shear layer. This behaviour is the result a minor, well understood vibration of the wind tunnel caused by the flying-hot-wire propulsion system. By deliberately forcing the shear layer instability with a periodic input, it was possible to overwhelm these effects and obtain smooth streamlines. This is demonstrated by figure 17 which shows the equivalent pattern when the flow is forced.

In both cases the streamlines emanating from the front and rear sides of the jet form open bifurcation lines with respect to the cross-flow and jet fluid. Examination of the volume flux between streamlines emanating from the front and rear sides of the jet indicates that in both cases there is a considerable flow of jet fluid away from the centre-plane in the mean. Also, the forced jet appears to bend more sharply than the unforced jet, which may be due to enhanced mixing in the shear layer, brought about by the forcing of the shear layer roll-up. The downward curvature of the streamlines

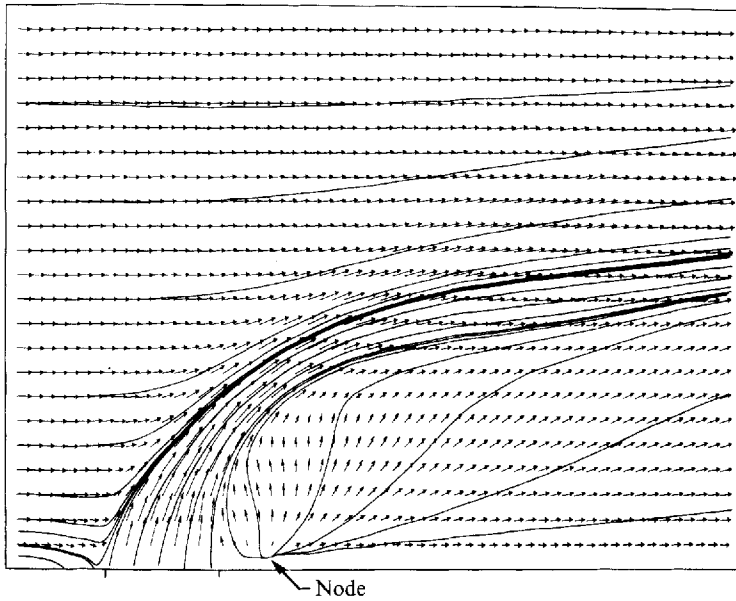


FIGURE 17. Time-averaged vector field and streamline pattern in the vertical centre-plane for the forced jet. $Re = 6200$, $R = 2.2$ and $\delta/D = 0.28$. The pipe location is indicated by tick marks.

near the floor ahead of the jet is broadly consistent with the streakline patterns shown in the previous section of this paper.

Downstream of the jet, in both the unforced and forced cases, there appears to be a node which resides a short distance downstream of the edge of the nozzle and above the flat wall. The displacement above the wall is most clearly shown in the forced results. Recall that an extra row of experimental data, mid-way between the flat wall and the first level, was used to compute this pattern. Low Reynolds number flow visualization studies in the water channel confirmed that a node exists above the flat wall downstream of the jet. A numerical simulation of a jet in cross-flow by Sykes *et al.* (1986) also showed a node downstream of the jet, although it was located at the flat wall. The simulation, however, used a free-slip boundary condition at the flat wall and took no account of the flat-wall boundary layer.

Figure 18 shows the time-averaged pattern in the horizontal plane at $y = 40$ mm ($y/D = 0.42$) combined with the time-averaged pattern in the vertical centre-plane for the unforced case. The location of the pipe exit is indicated by a semi-circle. Some of the velocity data measured in the horizontal plane in the core region of the jet needed to be corrected for systematic errors due to yaw angle effects on the hot-wire probe. The correction scheme is described in Kelso (1991). It can be seen that the features in the sectional planes are consistent with each other. For example, downstream of the jet the fluid is swept horizontally towards the centre-line, forming a bifurcation line in the horizontal sectional plane. Consistent with this, sectional streamlines in the vertical plane show that fluid is swept towards the centre-line and then upwards, away from this horizontal plane.

The most important feature of figure 18 is the focus which is counter-clockwise and spirals out. It is difficult to judge the reliability of this feature because of the small number of grid points which define it. However, the existence of a vortex is in agreement with the flow visualization experiments in the water channel. The location

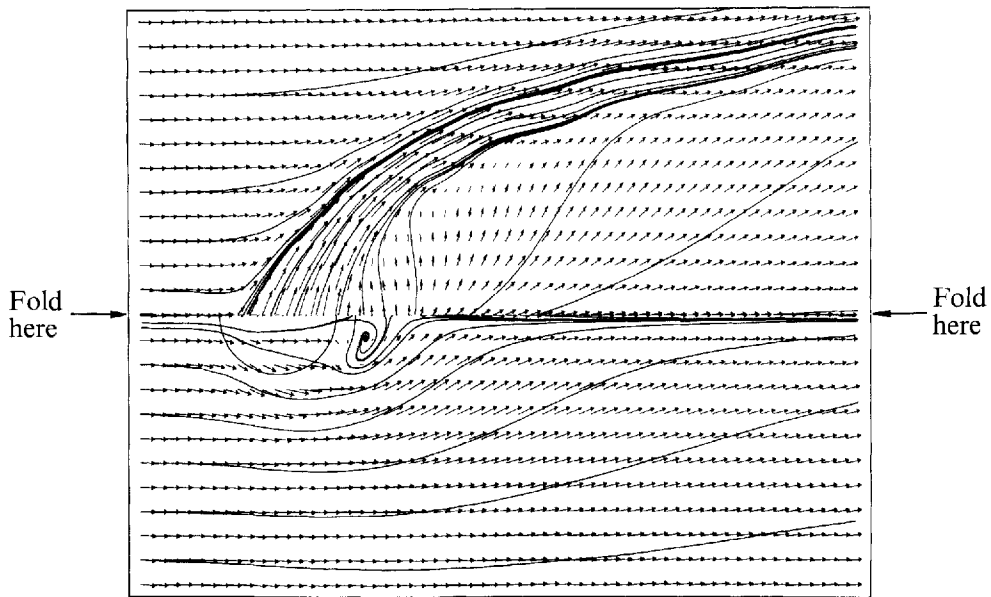


FIGURE 18. Composite vector field and streamline pattern for the unforced jet. The fold line lies at $y/D = 0.42$ and $z = 0$. $Re = 6200$, $R = 2.2$ and $\delta/D = 0.28$. The pipe location is indicated by a semi-circle.

of the focus relative to the pipe suggests that the focus is a feature of the wake region and is not produced by vorticity from the shear layer. It is probable that this feature is the time-average of the unsteady wake pattern, just as the time-average wake pattern of a circular cylinder or bluff plate is a pair of vortices in the near wake (see, for instance, Perry & Steiner 1987). The authors believe that this feature is the time-average of a wall vortex, which is part of the wake vortex system as described in §4 below.

The pattern shown in figure 18 suggests a lack of symmetry of the flow within the jet as indicated by a small spanwise (w -) velocity component on the centre-line at the downstream side. Although it is to be expected that some small w -velocity errors should be seen, the magnitudes of the measured velocities are in excess of any errors attributable to hot-wire drift or probe misalignment. The resulting pattern is therefore unsymmetrical. Surface pressure distributions measured by the authors support this conclusion. The lack of symmetry may have been due to inlet conditions at the intake of the jet.

Figure 19 shows the non-dimensionalized vorticity field ($\omega_n = \omega D/U_\infty$) calculated from the horizontal plane velocity field of figure 18. The vorticity associated with the wake region is clearly seen downstream of the jet exit. A vorticity peak also occurs close to where the shear layer from the pipe is located. It is of the same sign as the vorticity in the wake region, but about 60% of this peak value. This peak may represent the mean reorientation of the shear layer vorticity to initiate or contribute to the CVP as depicted in figure 9(b).

3.4.2. Forced structure

To obtain phase-averaged velocity measurements, the ring-like roll-up of the shear layer was forced by mechanically puffing the jet, thereby locking the roll-up process into a perfectly periodic cycle. In order to confirm qualitatively that this is a legitimate

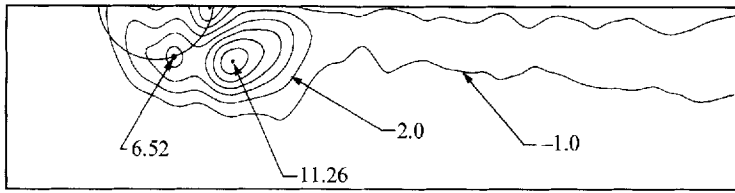


FIGURE 19. Non-dimensionalized phase-averaged vorticity contours for the horizontal cross-section at $y/D = 0.42$. Contours intervals are 2.0 units unless otherwise specified. Positive vorticity is anti-clockwise. $Re = 6200$, $R = 2.2$ and $\delta/D = 0.28$. The pipe location is indicated by a semi-circle.

forcing method which does not alter the appearance of the jet structure, the jet flow in the water channel was forced in a similar way at $R = 2.2$ and a Reynolds number of 1600. This was achieved by periodically squeezing the jet's supply tube at or close to the frequency of the unforced shear layer roll-ups. The conclusion of this simple test is that a moderate level of forcing appears to alter the growth rate of the ring vortices, but does not seem to affect the overall structure of the jet in cross-flow.

The meaningful representation of a phase-averaged velocity field is very difficult to achieve. The usual method used to interpret the topology of an eddy or a group of eddies is to observe the velocity field from a reference frame which is fixed relative to that eddy or that group. Cantwell & Coles (1983) and Steiner & Perry (1987) showed that this could be done successfully in the far wakes of bluff bodies. However, in a complex three-dimensional flow such as a jet in cross-flow, it is very difficult to interpret the local topology in the near field due to the large acceleration and growth rate of the eddies.

In the following discussion, the eddies (in figures 20 and 21) will be described as the upstream and downstream sides of three vortex rings. These will be referred to as ring 1 (closest to the pipe exit), ring 2 and ring 3 (furthest from the pipe exit).

Figure 20 shows plots of vorticity calculated from the phase-averaged velocity fields of phases 7 and 10 respectively. In these plots three distinct vortex pairs (i.e. rings) can be clearly identified as large concentrations of vorticity on the upstream and downstream sides of the jet. Close to the pipe exit, the vortex rings appear to be higher on the downstream side of the jet than on the upstream side. However, the upstream sides of the rings initially convect more rapidly than the downstream sides. Note the similarity between this plot and the dye visualization results, particularly figure 5(a) where the upstream side of the vortex ring (red) is initially lower than the downstream side of the ring (blue).

Note that the phase-averaged vorticity plots contain 'spurious' lumps of vorticity. These blemishes are believed to be the result of a minor vibration caused by the flying-hot-wire measurement system superimposed on the large-scale forced roll-up. The vorticity fields, being calculated from spatial derivatives of the velocity field, are extremely sensitive to this type of contamination. The phase-averaged vorticity fields are, in fact, surprisingly clean as the blemishes generally appear to be small compared with the vorticity peaks associated with the vortex rings. The upstream eddy of ring 2 in phase 10 is probably distorted by the contamination.

In order to determine from the phase-averaged velocity fields the actual topology of the shear layer structure on the vertical centre-plane, it is necessary to establish appropriate frames of reference, i.e. the convection velocity of each eddy. In this case the convection velocities were estimated from both the vortex celerity (Cantwell & Coles 1983) and the velocity corresponding to the location of the

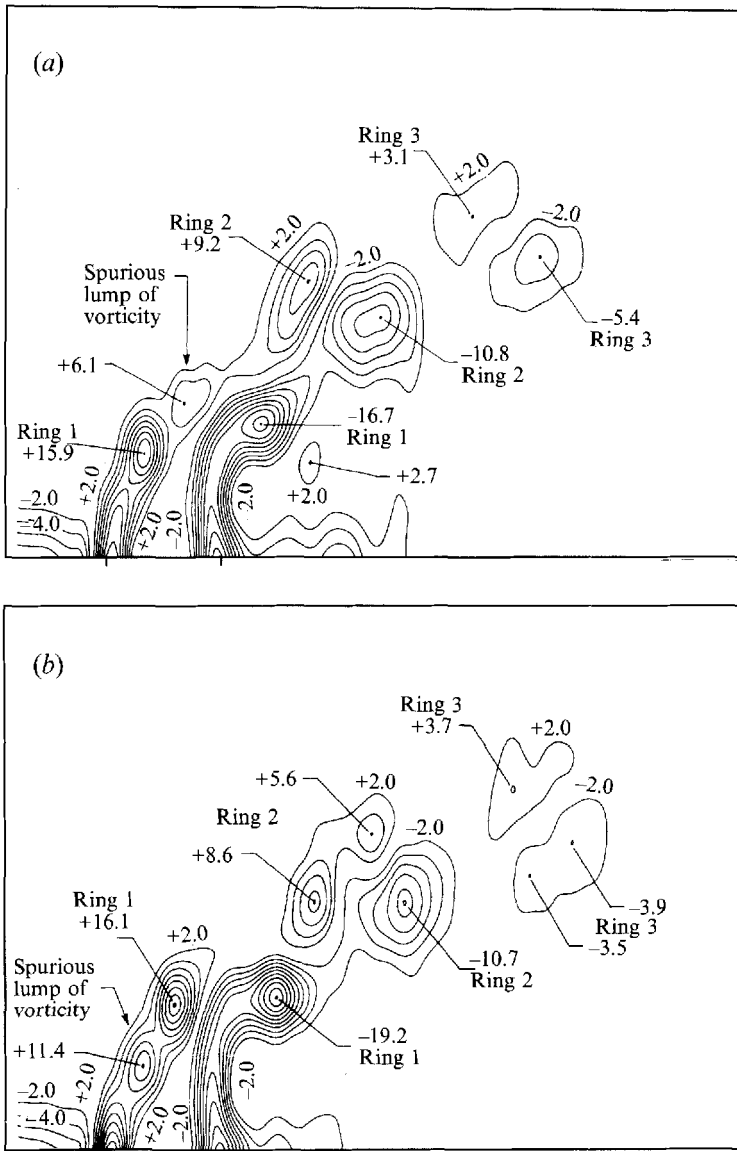


FIGURE 20. Non-dimensionalized phase-averaged vorticity contours for (a) phase 7 and (b) phase 10. Contours intervals are 2.0 units unless otherwise specified. Positive vorticity is anti-clockwise. $Re = 6200$, $R = 2.2$ and $\delta/D = 0.28$. The pipe location is indicated by tick marks.

centroid of vorticity of each eddy (centroidal velocity). On the whole, convection velocities estimated by the celerities and centroidal velocities are very similar. As expected, the convection velocities of the eddies vary widely over the velocity field (see Kelso 1991), so an examination of the topology of the velocity field must be done with care. When moving with an eddy to examine its topology, the flow field close to that eddy will become almost steady but the surrounding velocity field will not. Therefore, interpretations of topology must be confined to the close vicinity of the eddy which is steady relative to the moving observer.

Figure 21 shows the vector field and streamline patterns corresponding to figure 20(b) as seen by observers moving at different velocities. The positions of the vorticity centroids of the 'stationary' eddies are indicated by the intersection of two lines. In figure 21(a) it can be seen that the downstream eddy of ring 1 is the only clearly defined flow feature as the rest of the pattern is moving relative to this observer. In figure 21(b) the downstream eddies of rings 1 and 2 are evident although they are not correctly represented because they, too, are moving relative to this observer.

4. Surface and sectional flow structure

In order to obtain a flow case in which little or no unsteadiness occurred in the wake region (i.e. the 'upright vortices' were not yet forming), the Reynolds number and the velocity ratio were set to approximately 440 and 6.0 respectively. This allowed the detailed examination of the surface and wake flow structure without the problems associated with unsteadiness. The authors suggest that under these conditions the surface flow pattern and wake structure are likely to be topologically similar to the time-average of the flow patterns obtained over all the flow conditions discussed in this paper.

Figure 22(a) shows a plan view of the flow pattern obtained when filaments of dye are introduced into the cross-flow (above the flat wall) from far upstream of the jet. The dye is swept around the outside of the jet and inwards towards the centre-line, whereupon it wraps around a pair of streamwise vortices which trail downstream adjacent to the flat wall. These are the wall vortices as defined in figure 1 and they form part of the wake vortex system. The positions of the filaments of dye were chosen such that some dye convected downstream along the wall vortices and some convected upstream towards the jet along the wall vortices. A similar pattern (with one wall vortex marked) can be seen in elevation in figure 22(b). In this photograph dye was also injected from the dye injection port at the front of the pipe to show the relationship between the jet shear layer and the wall vortices. Surface dye visualization studies (not shown) confirm that the wall vortices are the result of the separation of the flat-wall boundary layer and therefore contain vorticity originating from the flat wall. As can be seen in figure 22, the wall vortices lift away from the flat wall and up into the rear side of the jet to merge with the CVP of the jet shear layer. In this way, vorticity from the flat-wall boundary layer is continuously fed into the CVP. Thus the vorticity contained in the CVP originates not only from the pipe wall, but also from the flat wall.

The existence of the wall vortices has also been noted by authors such as Wu *et al.* (1988) (who called them 'wake' vortices) although their origin and connection with the rest of the flow structure was not understood. The wall vortex patterns shown in figure 22 appear to be a steady equivalent of the unsteady vortices produced by the 'separation events' described by Fric & Roshko (1989, 1994) and Fric (1990). These authors suggested that the boundary layer separates owing to an adverse pressure gradient on the downstream side of the jet. Pressure distribution measurements conducted in the wind tunnel by the present authors (see Kelso 1991) as well as other authors such as Kavsaoglu & Schetz (1989) confirm that a strong adverse pressure gradient exists on the flat wall downstream of pressure minima located on either side of the pipe. These pressure minima occur at approximately $\pm 120^\circ$ from the upstream side of the pipe in the case of $R = 2.2$ and at smaller angles at higher velocity ratios.

Some additional observations are shown in figure 23. Here the dye was introduced into the flat-wall boundary layer upstream of the horseshoe vortex system on the far

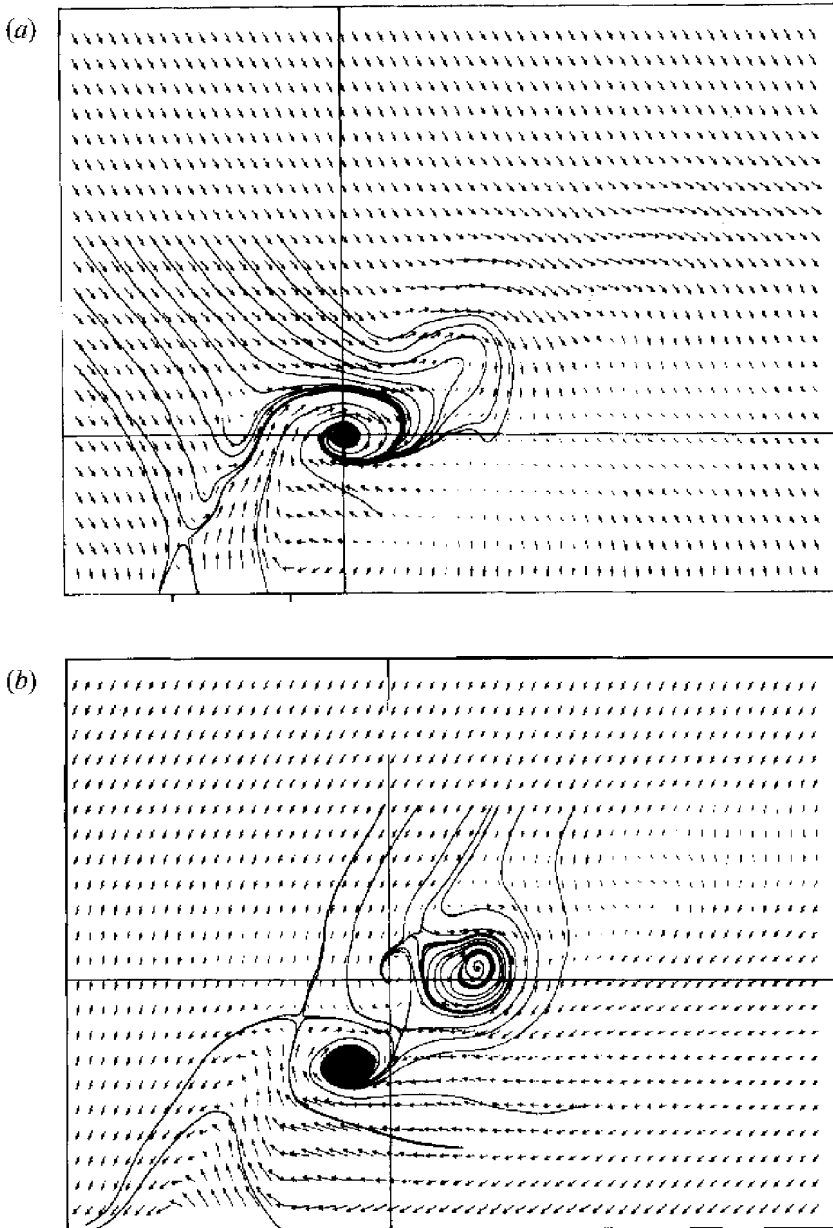


FIGURE 21. Instantaneous velocity fields and streamline patterns for phase 10 as seen by observers moving with (a) the celerity of the downstream eddy of ring 1 ($U_c = 0.582$, $V_c = 0.698$) and (b) the centroidal velocity of the upstream eddy of ring 2 ($U_c = 1.30$, $V_c = 0.60$). The intersection of the 'cross hairs' indicates the steady eddy. $Re = 6200$, $R = 2.2$ and $\delta/D = 0.28$. The pipe location is indicated by tick marks.

side of the centre-plane, whereupon it was convected around the jet and towards the rear side. From here the dye was lifted away from the wall at two locations, both of which give the appearance of tornado-like critical points or complex-eigenvalue critical points. The upstream tornado was probably fed by the spanwise dye slot shown in figure 22(a). The dye that is lifted away from the flat wall at these critical

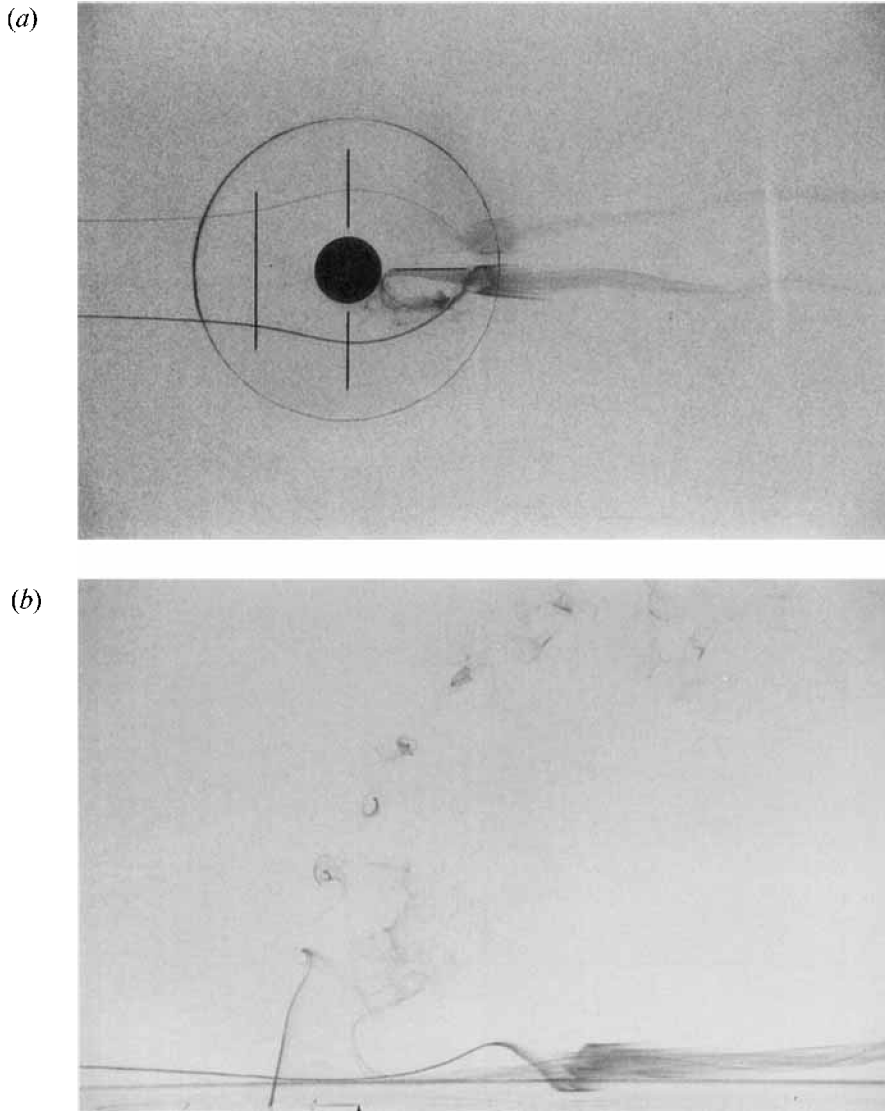


FIGURE 22. Steady wall vortex pattern obtained at $Re = 440$, $R = 6.0$ and $\delta/D = 1.3$, visualized by filaments of dye introduced far upstream. (a) Plan view, (b) elevation view. In (b) the location of the pipe is indicated by dye injected from the dye injection port at the upstream edge and an arrow head at the downstream edge.

points is entrained into the CVP roll-up of the jet shear layer. Our observations suggest that these features are connected (somehow) to the wall vortices and they are also locations where flat-wall vorticity is lifted away from the wall to merge ultimately with the CVP.

From these and many other detailed observations of dye traces a series of conjectured flow patterns have been constructed. These patterns describe the low Reynolds number flow case currently being discussed and also seem to fit the time-averaged observations over the range of Reynolds numbers and velocity ratios studied in this paper. The conjectured surface streamline pattern on the flat wall combined with the

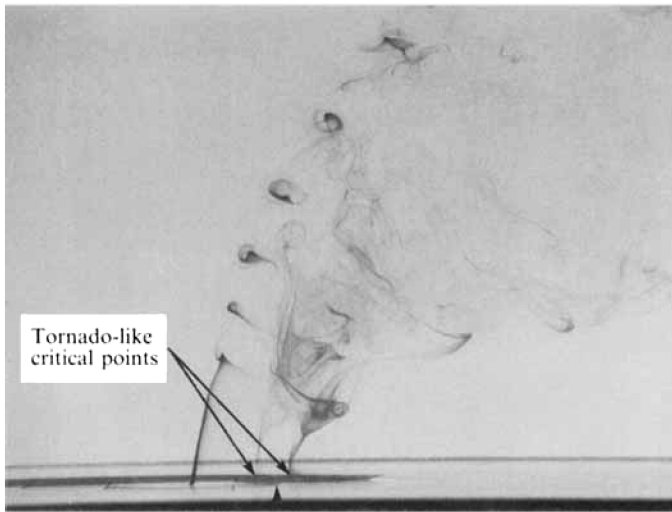


FIGURE 23. Flow pattern obtained when dye, which is introduced ahead of the horseshoe vortex system, is swept to the rear side of the jet. Here it is lifted away from the flat wall at complex-eigenvalue critical points. The location of the pipe is indicated by dye released from the dye injection port below the upstream lip and an arrow head at the downstream lip. $Re = 440$, $R = 6.0$ and $\delta/D = 1.3$.

conjectured streamline pattern in the vertical centre-plane are given in figure 24. No apologies are made for any scaling errors or distortion of the pattern as the aim here is to describe the flow topology only. Some of the features shown on the flat wall bear similarity to the observations of Krothapalli *et al.* (1990) and Foss (1980).

Upstream of the jet exit on the flat wall (x, z -plane), where the horseshoe vortex system is formed, the surface flow pattern consists of a series of positive and negative bifurcation lines. These bifurcation lines lie around the front and sides of the jet, converging towards the rear of the jet and spiralling into a focus (complex-eigenvalue critical point A) adjacent to the rear side of the jet. A second focus (complex-eigenvalue critical point B) is shown upstream of A. This point lies close to the location where the bifurcation line of the separation (within the pipe) leaves the pipe as shown in figure 11. These complex-eigenvalue critical points are locations where fluid spirals in and is lifted away from the flat wall (see figure 23). On the downstream side of the jet, the flow pattern on the flat wall consists of a node on the centre-line (C) with saddles on either side. Bifurcation lines, on which these saddles lie, extend downstream.

The surface streamline pattern inside the pipe (see figure 11) can be interpreted similarly and related to the rest of the flow pattern. In this pattern a node is indicated at the upstream edge of the pipe. This node as is also identified in figure 24. The presence of a second separation at the upstream edge of the pipe, as described in figure 14, has been neglected deliberately as it would only affect the topology in the immediate vicinity of the node. In the large, the pattern would be as shown in figures 11 and 24. On the downstream side of the pipe interior at $\theta = 180^\circ$, the surface streamlines diverge, indicating a positive bifurcation line. This is consistent with the saddle point indicated in figure 24.

The vertical centre-plane in figure 24 contains features which have been discussed earlier, including node G downstream of the jet which was inferred from

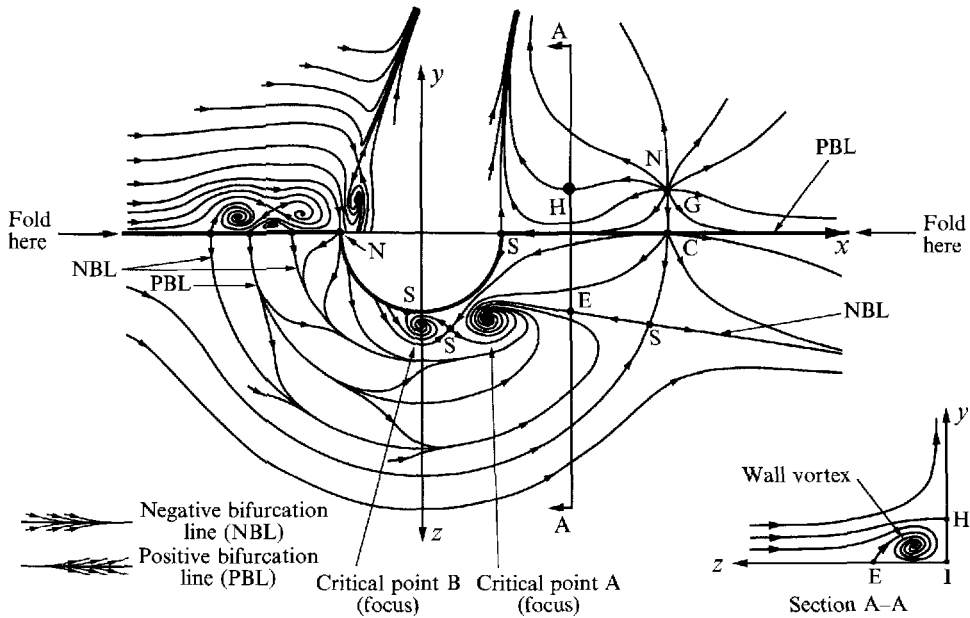


FIGURE 24. Composite streamline pattern. The horseshoe vortices are not included in section A-A. S denotes a saddle point and N denotes a node on the flat wall (x, z -plane) and centre-plane (x, y -plane).

topological arguments and confirmed experimentally by dye visualization. Figure 24 also shows a transverse cross-section of this flow on a sectional plane A-A (parallel to the y, z -plane) between node C and the downstream edge of the pipe. The location of one wall vortex is shown and the horseshoe vortices have been deliberately omitted. The separation point E in section A-A corresponds to the negative bifurcation line on the flat wall. The saddle point I corresponds to the positive bifurcation line on the centre-line (x -axis). The saddle point H above the flat wall corresponds to a locally horizontal ($v = 0$) streamline emanating from node G.

5. Unsteady wake structure: the occurrence of upright vortices

In §4, the structure of the wake region was described for the case of $Re = 440$ and $R = 6.0$ and the wall vortices were identified and shown to originate at the flat wall. It was also shown that the wall vortices seem to merge with the CVP immediately behind the pipe exit as shown in figure 22. However, when the Reynolds number is increased, the wake region develops unsteady vortices which we call the 'upright vortices' (see figure 1). Upright vortices are variously referred to in the literature as 'wake vortices' (Fric & Roshko), 'spinoff vortices' (Wu *et al.* 1988) and 'zipper vortices' (Morton & Ibbetson 1994). In figure 25, where $Re = 1600$ and $R = 4.0$, upright vortices are apparent in the wake and appear to be joined to the wall vortices and also ultimately merge with the CVP. Under these conditions, the upright vortices are shed irregularly or aperiodically with the vortex cores, as marked by the dye, being generally slender with respect to the jet diameter. A typical close-up view of the wake region is given in figure 25(b), which shows a vortex similar to a wall vortex (see arrow) lifting away from the flat wall.

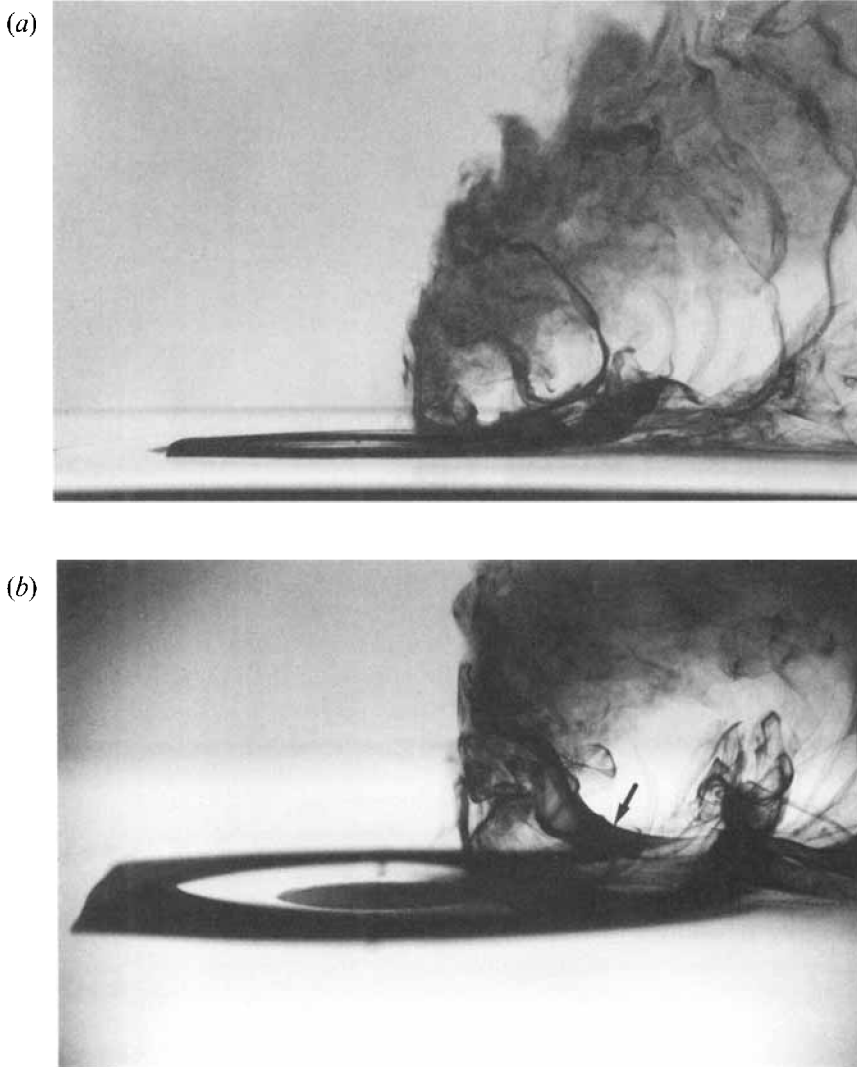


FIGURE 25. Flow patterns obtained when dye is introduced from a slit in the flat wall at $Re = 1600$, $R = 4.0$ and $\delta/D = 0.61$: (a) and (b) show the same flow at different times and different magnification. The arrow in (b) points to a vortex lifting away from the flat wall.

Figure 26 (see p. 119) shows the wake region at a $Re = 2700$ and $R = 4.0$. These conditions were chosen on the basis of our observations that the shedding of the upright vortices becomes more regular with increasing Reynolds number and when the velocity ratio exceeds approximately 3. Under these conditions the upright vortices are more periodic and larger in scale and the vortex roll-up process involves the periodic oscillation of the entire jet flow pattern. This oscillation results in critical point A oscillating back-and-forth in the streamwise (x) direction from the relative position shown in figure 24 to immediately downstream of (or even merged with) critical point B. In figure 26, red and blue dyes were injected from the radial slits in the jet mounting disc. Here the jet mounting disc (see figure 2) was rotated by 45° , and the slits at $\pm 45^\circ$ from the centre-line on the downstream side of the jet were used

to mark the boundary layer fluid. In doing this, blue dye was introduced ahead of the location where the flat-wall boundary layer separated on the near side, with red dye introduced similarly on the far side. It was noted that most, if not all, blue upright vortices appeared to occur on the near side of the wake, with analogous behaviour of the red vortices. Occasionally, upright vortices were marked by a mixture of red and blue dyes. Figure 26(a) shows a flow regime where alternating red and blue upright vortices occur. Figure 26(b) shows a photograph taken a short time later under the same flow conditions, where the upright vortices occur in pairs of red followed by pairs of blue-marked vortices. The two patterns shown here were observed regularly at these flow conditions with the vortex orientation changing intermittently from one pattern to another. The pattern shown in figure 26(a) is the most commonly occurring.

Flow visualization studies performed by Fric & Roshko (1989, 1994) and Fric (1990) also suggest that at high Reynolds number the upright vortex orientation may change from one pattern to another. Comparison of figure 6(b) of Fric & Roshko (1994) (figure 5.2 of Fric 1990, figure 6 of Fric & Roshko 1989) with other similarly obtained photographs shows that two distinct patterns may be occurring. Figure 27(a) shows a 'cartoon' of the typical horizontal cross-sectional flow pattern for all velocity ratios ($R = 2, 4, 6, 8$ and 10) shown by Fric & Roshko. This pattern is similar to the classical von Kármán vortex street, with vortices alternating in circulation, and seems to be the most commonly occurring. Figure 27(b) shows a 'cartoon' of the horizontal cross-sectional flow pattern presented in figure 6(b) of Fric & Roshko (1994). It shows the upright vortex pattern to consist, in this particular case, of mushroom-like structures where the vortices appear to be grouped into pairs of opposite circulation, in contrast to the classical von Kármán pattern. It may be possible for a von Kármán vortex street to evolve into such a configuration, but this is unlikely to occur over such a short distance. Note that these authors do not comment on the difference between the two flow patterns discussed here.

Figure 28 shows three alternative mechanisms which may explain the observations depicted in figures 26 and 27. These scenarios are based on our observations that, when the wake is unsteady, the upright vortices are 'shed' versions of the wall vortices. As was mentioned earlier, the 'wake' of a jet in cross-flow is not a wake in the conventional sense, since, as pointed out by Morton & Ibbetson (1994), it is unlikely to have any deficiency in momentum in the mean sense at least arising from the jet itself, i.e. it cannot be regarded as a drag-producing obstacle (such as a solid cylinder) and any momentum and total pressure deficit would probably arise from the flat-wall boundary layer and dissipation as suggested by Fric & Roshko (1994). Hence the vortex configurations for the various streets must have the property of not giving a mean momentum deficit.

A mechanism leading to upright vortex formations of the classical von Kármán type is described by figure 28(a). This would give the appearance of the vortices forming alternately on one side then the other. If this scenario is correct, all upright vortices of the same sign would be marked the same colour in the present experiment. Figure 28(b) depicts a similar mechanism where the upright vortices convect downstream in successive pairs from each side of the wake, leading to the formation of a mushroom-like pattern. If this mechanism is correct, in the present experiment each mushroom would be composed of vorticity, hence dye, from both sides of the wake. Therefore, each mushroom would consist of one red vortex and one blue vortex. Figure 28(c) describes a mechanism leading to mushroom-like structures where the upright vortices are formed by vortex loops on either side of the wake. If

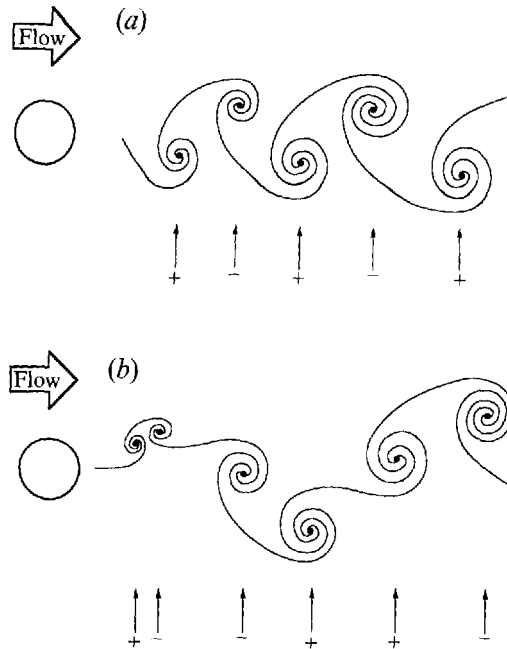


FIGURE 27. Authors' interpretation of streakline patterns corresponding to the smoke patterns shown in Fric (1990) and Fric & Roshko (1989, 1994). (a) Interpretation of typical horizontal cross-section streakline patterns of Fric & Roshko; (b) interpretation of figure 6(b) of Fric & Roshko (1994) for $R = 4.0$, $Z/D = 0.5$, $Re = 11400$. Note: + and - signs indicate sign of eddy circulation.

this scenario is correct, each mushroom would be composed of vorticity from one or the other side of the wake, leading to the mushrooms being marked all red or all blue in the present experiment. Further mechanisms have been proposed (e.g. Kelso, Delo & Smits 1993) and all are currently under investigation.

6. Conclusions

One can see that a kaleidoscope of phenomena exists for jets in cross-flow even for the simple case of the pipe outlet being flush with the wall. So far, in spite of its complexities, we have a broad understanding of the flow structure. Flow visualization in the water channel and flying-hot-wire measurements and smoke visualization in the wind tunnel have combined to give a fairly complete picture and critical point theory seems to be useful in interpreting these results. The results show that jets in cross-flow contain many vortex systems, all of which are somehow connected. It is clear that the separation pattern inside the pipe is important in the initial roll-up of the CVP. The vortex rings in the jet shear layer appear to tilt and bend such that they contribute a component of vorticity to the CVP. Vorticity from the flat wall also seems to contribute to the CVP by way of the wall vortices and the complex-eigenvalue critical points on the flat wall. Vortex breakdown appears to be occurring in the CVP near the pipe outlet. The upright vortices in the wake come from the vorticity generated at the flat wall and this vorticity somehow links up with the wall vortices and the CVP. Some alternative mechanisms for the shedding of the upright vortices in the wake have been suggested. The horseshoe vortex system seems to play only a minor role in the overall structure. Although it is difficult to summarize in a precise

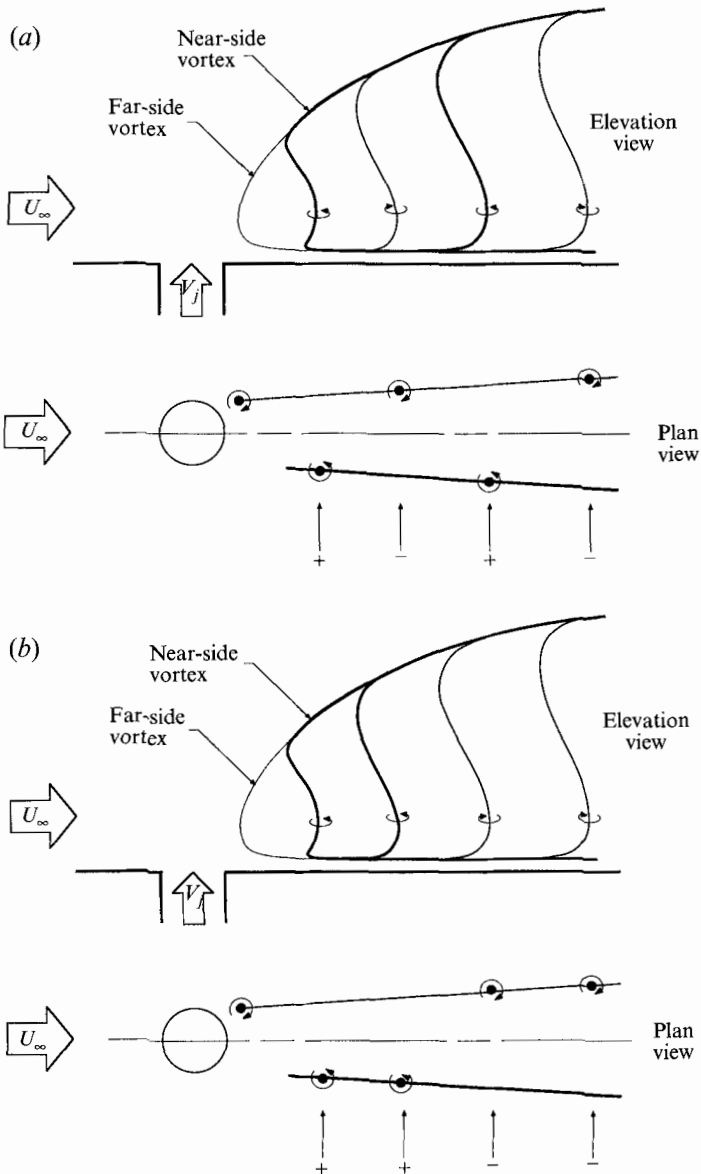


FIGURE 28. For caption see facing page.

manner how all of the disparate observations fit together, the authors have attempted to summarize the relationship between the various phenomena in figure 29 which shows a tentative sketch in (R, Re) -space. To complete the picture, some additional observations have been included for the $R < 2$ region.

The authors feel that most of the salient features on the surface of the pipe and the flat wall and the general flow structure surrounding the jet itself have been described adequately in broad geometrical and topological terms. Perhaps direct numerical simulations at low Reynolds numbers may shed some light on the features which are difficult to resolve experimentally. Although low Reynolds number flows have been discussed in this paper, the authors believe that the global topological features

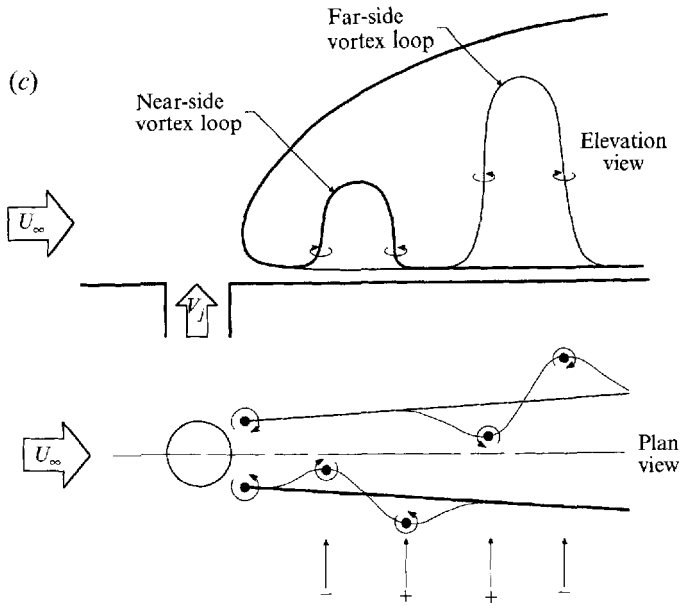


FIGURE 28. Three proposed mechanisms leading to the upright vortices in the wake. (a) A mechanism leading to a pattern similar to a von Kármán vortex street. (b) A mechanism leading to mushroom-like upright vortex structures. (c) Alternative mechanism leading to mushroom-like upright vortex structures.

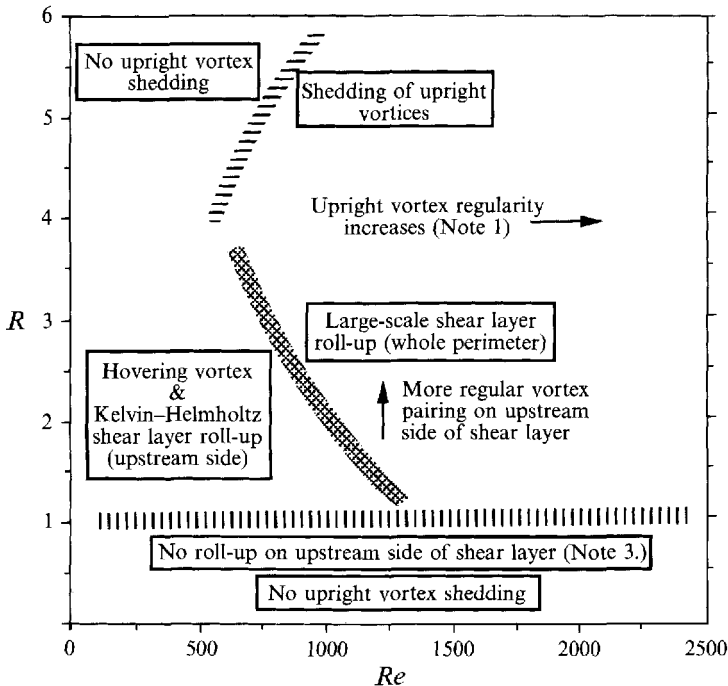


FIGURE 29. Graphical summary of jet in cross-flow phenomena, showing the range of phenomena and the R, Re -ranges for which they occur. The precise shapes of the zone boundaries are unknown. Note 1: Most regular upright vortex shedding at $R \approx 4$; note 2: vortex breakdown at $R > 3$; note 3: see Lim, Kelso & Perry (1992)

described here apply to higher Reynolds number flows with velocity ratios between 2.0 and 6.0. The correspondence between the lower Reynolds number instantaneous dye patterns ($440 \leq Re \leq 2700$ and $2.0 \leq R \leq 6.0$) and the higher Reynolds number ($Re = 6200$ and $R = 2.2$) time-averaged wind tunnel measurements supports this suggestion. Comparison with the general body of literature supports this suggestion also.

The authors wish to acknowledge the financial assistance of the Australian Research Council. The first author acknowledges the support of the CSIRO and the Defence Science and Technology Organisation.

REFERENCES

- ANDREOPOULOS, J. 1982 Measurements in a jet-pipe flow issuing perpendicularly into a cross stream. *Trans. ASME I: J. Fluids Engng* **104**, 493–499.
- ANDREOPOULOS, J. 1984 Initial conditions, Reynolds number effects and the near field characteristics of the round jet in a cross flow. *J. Flight Sci. Space Res.* **8** Heft 2.
- ANDREOPOULOS, J. 1985 On the structure of jets in crossflow. *J. Fluid Mech.* **157**, 163–197.
- ANDREOPOULOS, J. & RODI, W. 1984 Experimental investigation of jets in a cross flow. *J. Fluid Mech.* **138**, 93–127.
- BAKER, C. J. 1980 The turbulent horseshoe vortex. *J. Wind Engng Ind. Aero.* **6**, 9–23.
- BERGELES, G., GOSMAN, A. D. & LAUNDER, B. E. 1976 The near-field character of a jet discharged normal to a main stream. *Trans. ASME C: J. Heat Transfer* **98**, 373–378.
- BRADBURY, L. J. S. & WOOD, M. N. 1965 The static pressure distribution around a circular jet exhausting normally from a plane wall into an airstream. *Conf. Proc.* 822. British Aeronautical Research Council, London, UK.
- BROADWELL, J. E. & BREIDENTHAL, R. E. 1984 Structure and mixing of a transverse jet in incompressible flow. *J. Fluid Mech.* **148**, 405–412.
- CANTWELL, B. & COLES, D. 1983 An experimental study of entrainment and transport in the turbulent near wake of a circular cylinder. *J. Fluid Mech.* **136**, 321–374.
- CHASSAING, P., GEORGE, J., CLARIA, A. & SANANES, F. 1974 Physical characteristics of subsonic jets in a cross stream. *J. Fluid Mech.* **62**, 41–64.
- COELHO, S. L. V. & HUNT, J. C. R. 1989 The dynamics of the near field of strong jets in crossflows. *J. Fluid Mech.* **200**, 95–120.
- CRABB, D., DURAO, D. F. G. & WHITELAW, J. H. 1981 A round jet normal to a crossflow. *Trans. ASME I: J. Fluids Engng* **103**, 142–153.
- DOLIGALSKI, T. L., SMITH, C. R. & WALKER, J. D. A. 1994 Vortex interactions with walls. *Ann. Rev. Fluid Mech.* **26**, 573–616.
- FEARN, R. & WESTON, R. P. 1974 Vorticity associated with a jet in a cross flow. *AIAA J.* **12**, 1666–1671.
- FOSS, J. F. 1980 Interaction region phenomena for the jet in a cross-flow problem. *Rep. SFB 80/E/161*. University of Karlsruhe.
- FRIC, T. F. 1990 Structure in the near field of the transverse jet. PhD thesis, California Institute of Technology.
- FRIC, T. F. & ROSHKO, A. 1989 Structure in the near field of the transverse jet. *Seventh Symposium on Turbulent Shear Flows*, pp. 6.4.1–6.4.6.
- FRIC, T. F. & ROSHKO, A. 1994 Vortical structure in the wake of a transverse jet. *J. Fluid Mech.* **279**, 1–47.
- GOLDSTEIN, J. E. & SMITS, A. J. 1994 Flow visualization of the three-dimensional, time-evolving structure of a turbulent boundary layer. *Phys. Fluids* **6**, 577–587.
- GURSUL, I., LUSSEYRAN, D. & ROCKWELL, D. 1990 On interpretation of flow visualization of unsteady shear flows. *Exps. Fluids* **9**, 257–266.
- HORNUNG H. & PERRY A. E. 1984 Some aspects of three-dimensional separation, Part 1. Stream-surface bifurcations. *Z. Flugwiss Weltraumforsch.* **8**, 77–87.

- KAMOTANI, Y. & GREBER, I. 1972 Experiments on a turbulent jet in a cross flow. *AIAA J.* **10**, 1425–1429.
- KAVSAOGLU, M. S. & SCHETZ, J. A. 1989 Effects of swirl and high turbulence on a jet in a crossflow. *J. Aircraft* **26**, 539–546.
- KEFFER, J. F. & BAINES, W. D. 1963 The round turbulent jet in a cross-wind. *J. Fluid Mech.* **15**, 481–496.
- KELSO, R. M. 1991 A study of free shear flows near rigid boundaries. PhD thesis, University of Melbourne.
- KELSO, R. M., DELO, C. & SMITS, A. J. 1993 Unsteady wake structures in transverse jets. *AGARD-CP* 534, Paper 4.
- KELSO, R. M., LIM, T. T. & PERRY, A. E. 1989 A new flying hot-wire for flow topology studies. *Proc. 10 AFMC*, pp. 5.5–5.8.
- KELSO, R. M., LIM, T. T. & PERRY, A. E. 1994 A novel flying hot-wire system. *Exps. Fluids* **16**, 181–186.
- KELSO, R. M. & SMITS, A. J. 1995 Horseshoe vortex systems resulting from the interaction between a laminar boundary layer and a transverse jet. *Phys. Fluids* **7**, 153–158.
- KROTHAPALLI, A., LOURENCO, L. & BUCHLIN, J. M. 1990 Separated flow upstream of a jet in a crossflow. *AIAA J.* **28**, 414–420.
- KROTHAPALLI, A. & SHIH, C. 1993 Separated flow generated by a vectored jet in crossflow. *AGARD-CP* 534, Paper 5.
- KUZO, D. M. & ROSHKO, A. 1984 Observations on the wake region of the transverse jet. *Bull. Am. Phys. Soc.* **29**, 1536.
- LIGHTHILL, M. J. 1963 In *Laminar Boundary Layers* (ed. L. Rosenhead). Oxford University Press.
- LIM, T. T., KELSO, R. M. & PERRY, A. E. 1992 A study of a round jet in cross-flow at different velocity ratios. *Proc. 11th Australasian Fluid Mechanics Conf., Hobart, Australia*, pp. 1089–1092.
- MCMAHON, H. M., HESTER, D. D. & PALFREY, J. G. 1971 Vortex shedding from a turbulent jet in a cross-wind. *J. Fluid Mech.* **48**, 73–80.
- MCMAHON, H. M. & MOSHER, D. K. 1969 Experimental investigation of pressures induced on a flat plate by a jet issuing into a subsonic crosswind. Analysis of a jet in a subsonic crosswind. *NASA SP* 218, pp. 49–62.
- MORTON, B. R. 1984 The generation and decay of vorticity. *Geophys. Astrophys. Fluid Dyn.* **28**, 277–293.
- MORTON, B. R. & IBBETSON, A. 1994 Jets deflected in a crossflow. *Proc. Intl Colloquium on Jets, Wakes and Shear Layers, CSIRO DBCE, Melbourne, Australia, April 18–20*.
- MOUSSA, Z. M., TRISCHKA, J. W. & ESKINAZI, S. 1977 The near field in the mixing of a round jet with a cross-stream. *J. Fluid Mech.* **80**, 49–80.
- PATANKAR, S. V., BASU, D. K. & ALPAY, S. A. 1977 Prediction of the three-dimensional velocity field of a deflected turbulent jet. *Trans. ASME I: J. Fluids Engng* **99**, 758–762.
- PERRY, A. E. & CHONG, M. S. 1987 A description of eddying motions and flow patterns using critical-point concepts. *Ann. Rev. Fluid Mech.* **19**, 125–155.
- PERRY, A. E. & FAIRLIE, B. D. 1974 Critical points in flow patterns. *Adv. Geophys. B* **18**, 299–315.
- PERRY, A. E. & LIM, T. T. 1978 Coherent structures in coflowing jets and wakes. *J. Fluid Mech.* **88**, 451–463.
- PERRY, A. E., LIM, T. T. & CHONG, M. S. 1980 The instantaneous velocity fields of coflowing jets and wakes. *J. Fluid Mech.* **101**, 243–256.
- PERRY, A. E. & STEINER, T. R. 1987 Large-scale vortex structures in turbulent wakes behind bluff bodies. Part 1. Vortex formation processes. *J. Fluid Mech.* **174**, 233–270.
- PERRY, A. E. & TAN, D. K. 1984 Simple three-dimensional vortex motions in coflowing jets and wakes. *J. Fluid Mech.* **141**, 197–231.
- PRATTE, B. D. & BAINES, M. 1967 Profiles of the round turbulent jet in a crossflow. *J. Hydronaut. Div. ASCE* **92**, 53–64.
- RAJARANTNAM, N. & GANGADHARAIAH, T. 1983 vortex structure of circular jets in crossflow. *J. Wind Engng Indust. Aero.* **12**, 155–164.
- SCORER, R. S. 1958 *Natural Aerodynamics*. Pergamon Press.
- SHANG, J. S., McMASTER, D. L., SCAGGS, N. & BUCK, M. 1989 Interaction of jet in hypersonic cross stream. *AIAA J.* **27**, 323–329.

- STEINER, T. R. & PERRY, A. E. 1987 Large-scale vortex structures in turbulent wakes behind bluff bodies. Part 2. Far-wake structures. *J. Fluid Mech.* **174**, 271–298.
- SUCCEC, J. & BOWLEY, W. W. 1976 Prediction of the trajectory of a turbulent jet injected into a crossflowing stream. *Trans. ASME I: J. Fluids Engng* **98**, 667–673.
- SYKES, R. I., LEWELLEN, W. S. & PARKER, S. F. 1986 On the vorticity dynamics of a turbulent jet in a crossflow. *J. Fluid Mech.* **80**, 49–80.
- WU, J. W., VAKILI, A. D. & YU, F. M. 1988 Investigation of the interacting flow of nonsymmetric jets in crossflow. *AIAA J.* **26**, 940–947.